Submitted to the International Journal of Geomechanics

26th April 2016

TITLE:

A Fully Coupled THM Double Porosity Formulation for Unsaturated Soils

AUTHORS:

Marcelo Sánchez[1], Antonio Gens[2], Maria Victoria Villar[3] and Sebastiá Olivella[4]

AFFILIATIONS:

[1] Zachry Department of Civil Engineering, Texas A&M University, College Station, US. msanchez@civil.tamu.edu

[2] Department of Geotechnical Engineering and Geosciences, Universitat Politecnica de Catalunya, Barcelona, Spain. antonio.gens@upc.edu

[3] CIEMAT, Centro de Investigaciones Energéticas, Medioambientales y Tecnológicas, Madrid, Spain. mv.villar@ciemat.es

[2] Department of Geotechnical Engineering and Geosciences, Universitat Politecnica de Catalunya, Barcelona, Spain. sebastia.olivella@upc.edu

CORRESPONDING AUTHOR:

Dr Marcelo Sánchez
Associate Professor
Zachry Department of Civil Engineering
Texas A&M University
College Station Texas
77843-3136, USA
Telephone: (+1) 979 862 6604
Fax: (+1) 979 862 7696
E-mail: msanchez@civil.tamu.edu

Keywords: double porosity, unsaturated soils, THM coupled phenomena, compacted expansive clays, fabric/structure of materials, multiphase flow, nuclear waste disposal.

ABSTRACT

This work presents a fully coupled formulation developed to handle engineering problems in unsaturated (and saturated) soils that present two dominant void levels. The proposed framework assumes the presence of two porous media linked through a mass transfer term between them. In its more general form, the proposed approach allows the consideration of non-isothermal multiphase flow coupled with the mechanical problem. The double porosity formulation was implemented in a finite element code and it has been used to analyze a variety of engineering problems. The approach is especially suitable for cases in which the material exhibits a strong coupling between the mechanical and the hydraulic problems in both media, as for example swelling clays. For those types of problems the proposed formulation is used in conjunction with the mechanical double structure model already proposed by the authors. This paper presents the coupled formulation and the application of the proposed approach to problems involving expansive unsaturated clays. Very satisfactory results were obtained in these analyses.

INTRODUCTION

Often, saturated and unsaturated soils exhibit a double porosity. For example, in many compacted soils (especially when compacted on the dry side) the fabric is composed by an assembly of quasi-saturated aggregates forming a rather open structure that must be distinguished from the soil microstructure itself. Expansive clays typically exhibit a clear dual porosity with two dominant void sizes, namely: the macropores (or inter-aggregate voids) and the micropores (or intra-aggregates voids). In other cases, the double structure is directly related to the material manufacturing, for instance in seals composed of high-density clay-pellets (Fig. 1). The need to distinguish between different kinds of voids can also be found in other type of engineering problems involving fractured rocks and/or fissured soils, where the distinction between the pore levels associated with matrix and joints is necessary to achieve a good representation of the problem.

The analysis of problems like the ones listed above is generally performed using single porosity models, assuming average material properties over an elementary representative volume. However, such kind of approaches fall short in properly capturing the behavior of soil that exhibits a clear double porosity. In this paper, an existing fully coupled Thermo-Hydro-Mechanical (THM) formulation for single porosity media (Olivella et al., 1994) is extended to double porosity media with the aid of the double porosity theory (e.g. Barrenbaltt et al., 1960; Warren and Root, 196; Aifantis, 1980). Double porosity models consider the porous medium as two interacting continuous media coupled through a leakage term that controls the mass transfer between them. This simple idea allows extending many of the concepts and laws typically used in single porosity models to problems in which it is necessary to account for the different type of void levels present in the material.

75 The double porosity theory has been extensively used in different fields. The earlier
76 applications are related to the modelling of ground water and oil flow in fractured
77 reservoirs. Barrenblat et al. (1960) and Warren and Root (1963) used the double porosity
78 theory to model saturated flows in non-deformable media. Later on, this theory was
79 extended to deformable media by Aifantis (1980), and was widely used to model problems
80 involving deformable fractured/fissured porous media (e.g. Wilson and Aifantis, 1982;
81 Ellsworth and Bai, 1992; Musso and Federico, 1993; Bai et al., 1994; Ghafouri and Lewis,
82 1996; Khalili et al., 1999; Callari and Federico, 2000). The double porosity theory has been
83 extended to the case of multiphase flow, in particular to applications related to oil
84 production in fractured media (e.g. Lewis and Ghafouri, 1997). The effect of temperature
85 has also been considered in dual porosity media (e.g. Master et al., 2000, Khalili and
86 Selvadurai, 2003). The double porosity models have also been widely used to solve solute-
87 transport problems in which the matrix diffusion is a relevant phenomenon (e.g. Carrera et
88 al., 1997; Birkholzer et al., 2000). Double structure concepts have been used to describe the
89 mechanical behavior of swelling materials (Alonso et al., 1991, 1998; Hueckel, 1992; Gens
90 and Alonso, 1992; Sánchez et al., 2005, 2012.b; Mašín, 2013). More recently, Borja and
91 Koliji (2009) applied double porosity concepts and continuum principles of
92 thermodynamics to derive an expression for the effective stress tensor in multiphase
93 porous media displaying two porosity scales. The double porosity theory/concept has been
94 extensively used in the past. Therefore, the review presented above does not pretend to
95 cover all the published works in this subject.

96 Concerning the treatment of the mechanical problem, different assumptions have been
97 made in double porosity theories. For instance, in some problems the compressibility of

98 the fractured/fissured media was ignored and only the deformation of the matrix domain
99 was considered (e.g. Ghafouri and Lewis, 1996; Lewis and Ghafouri, 1997; Master et al.,
100 2000). Another common hypothesis considered when modeling the consolidation
101 processes in fractured or fissured materials is that the behavior of the whole medium is
102 elastic and average mechanical properties of the media are adopted (e.g. Wilson and
103 Aifantis, 1982; Ellsworth and Bai, 1992; Bai et al., 1994; Musso and Federico, 1993).
104 Previous double porosity formulations, and their applications, have been limited to elastic
105 media. The formulation presented in this work is capable of considering independent
106 mechanical constitutive laws models for each medium, including nonlinear and elasto-
107 plastic mechanical models. It is also able to consider unsaturated flow under non-
108 isothermal conditions. Special attention is paid to the incorporation of the hydro-
109 mechanical couplings in the governing equations. The proposed double porosity
110 formulation has been implemented in the finite element program CODE_BRIGHT
111 (Olivella et al., 1996), and it has been used to analyze a variety of problems, including the
112 behavior of unsaturated clay barriers and seals intended for the isolation of nuclear waste
113 using an advanced elasto-plastic mechanical model.

114 ## THEORETICAL FRAMEWORK

115 A good schematic representation of the double porosity concept is presented in Fig. 2a) for
116 the case of fractured/fissured porous media, where two overlapping continua are
117 distinguished: i) a porous medium '1', accounting for the discontinuities; and ii) a porous
118 medium '2', representing the porous matrix. The mass transfer between both sub-domains
119 is controlled by a leakage term. A similar conceptual model can be adopted for expansive
120 materials in which two different structure of pores can generally be distinguished (Fig.2b): a

121 medium '1', associated with the macro (or interaggregate) pores between the clay
122 aggregates, and ii) a medium '2' associated with the clay matrix.

123 The concepts described above have been used in this work to extend an existing fully
124 coupled *THM* formulation for single porosity media to deal with problems involving
125 materials presenting two porosity scales. The starting point is the *THM* formulation
126 proposed by Olivella et al. (1994) and the associated finite element program
127 CODE_BRIGHT. This formulation and code have been widely validated and satisfactorily
128 applied in different geo-engineering problems (e.g. Gens et al., 1998; 2009; Alonso et al.,
129 2005; Sánchez et al., 2012.a, 2011.b).

130 The main basic assumptions of the double porosity formulation presented in this paper are
131 summarized as follows:

132 • Two overlapping porous media have been considered, with the definitions of two
133 different global porosities:

$$a)\ \phi_1 = \frac{V_{v1}}{V}\ ; \qquad b)\ \phi_2 = \frac{V_{v2}}{V}\ ; \qquad c)\ \phi = \phi_1 + \phi_2 \tag{1}$$

134 where ϕ_1, ϕ_2, ϕ are the porosities related to medium 1, 2 and total, respectively.
135 V_{v1}, V_{v2} and V are the volume of voids medium 1, 2 and total, respectively.

136 • Fluid pressures, permeability, partial saturation and other properties can be
137 (separately) considered for each porous medium.

138 • Stress-small strain constitutive laws can be defined for each porous medium.

139 • Multiphase flow is considered for each domain.

140 • Mass transfer between the porous media is controlled through leakage terms.

- Thermal equilibrium between phases and media is assumed.
- The relevant *THM* phenomena are considered in a fully coupled way.
- The boundary conditions can be prescribed on both media.

It is also assumed that the porous media are made up of three phases: solid, liquid and gas. The liquid phase contains water and dissolved air whereas the gas phase is made up of dry air and water vapor. The problem is approached using a multi-phases, multi-species formulation that expresses mathematically the main coupled *THM* phenomena in terms of: balance equations, constitutive equations and equilibrium restrictions. In the following sections these three main components of the formulation are presented.

BALANCE EQUATIONS

The compositional approach was adopted to establish the mass balance equations. This implies that mass balances of species (rather than phases) are established. In this way the phase change terms do not appear explicitly in the governing equations (Olivella et al., 1994). The subscript identifies the phase (*s* for solid, *l* for liquid and *g* for gas), while the superscript indicates the species (*w* for water, and *a* for air). It has been assumed that the mineral coincides with the solid phase. The rest of the notation is indicated in notation.

SOLID MASS BALANCE EQUATION

The balance of the mineral can be expressed as (Olivella et al., 1994):

$$\frac{\partial}{\partial t}\left(\rho_s\left(1-\phi\right)\right)+\nabla\cdot\left(\rho_s\left(1-\phi\right)\dot{\mathbf{u}}\right)=0 \qquad (2)$$

where ρ_s is the solid density and $\dot{\mathbf{u}}$ is the solid velocity vector. A more convenient form of the balance equations is obtained considering the definitions of material derivate with respect to the solid velocity (i.e. Olivella et al., 1994):

$$\frac{D\phi}{Dt} = \frac{(1-\phi)}{\rho_s}\frac{D\rho_s}{Dt} + (1-\phi)\nabla.\dot{\mathbf{u}} = \frac{(1-\phi)}{\rho_s}\frac{D\rho_s}{Dt} + (1-\phi)\dot{\varepsilon}_v \tag{3}$$

where $\nabla.\dot{\mathbf{u}} = \dot{\varepsilon}_v$ is the increment of the total volumetric strain. This equation shows that the variation of porosity in time is related to the porosity changes induce by the variations in solid density, plus the porosity variations caused by volumetric deformation of the soil skeleton. Considering Eq. (1c) and assuming that the total volumetric strain can be written as the sum of contributions from each medium (i.e. $\dot{\varepsilon}_v = \dot{\varepsilon}_{v1} + \dot{\varepsilon}_{v2}$), Eq. (3) can be expressed as:

$$\frac{D\phi}{Dt} = \frac{D\phi_1}{Dt} + \frac{D\phi_2}{Dt} = \frac{(1-\phi)}{\rho_s}\frac{D\rho_s}{Dt} + (1-\phi_1-\phi_2)\left(\dot{\varepsilon}_{v1} + \dot{\varepsilon}_{v2}\right) \tag{4}$$

WATER MASS BALANCE EQUATION

Applying double porosity concepts, the water mass balance equation for each medium *j* (*j*=1,2) can be expressed as:

$$\frac{\partial}{\partial t}\left(\theta^w_{lj} S_{lj}\phi_j + \theta^w_{gj} S_{gj}\phi_j\right) + \nabla.\left(\mathbf{j}^w_{lj} + \mathbf{j}^w_{gj}\right) + (-1)^{j+1}\Gamma^w = f^w_j \qquad j = 1,2 \tag{5}$$

where θ^w_{lj} and θ^w_{gj} are the mass of water per unit volume of liquid and gas phases of medium *j*; $S_{\alpha j}$ is the volumetric fraction of the pore volume occupied by the α phase (α=*l*,

173 *g*) in medium *j*; $\mathbf{j}_{lj}^{w}$ and $\mathbf{j}_{gj}^{w}$ denote the total mass fluxes of water in the liquid and gas phases
174 in medium *j* with respect to a fixed reference system; f_j^w is the external mass supply of water
175 per unit volume of medium *j;* and Γ^w is the term related to the mass exchange term
176 between the two porous media. A quasi-steady model (e.g. Huyakorn, 1983) was adopted in
177 this work for the mass transfer term, as follows:

$$\Gamma^w = \gamma\left(P_{l1} - P_{l2}\right) \tag{6}$$

178 where γ is the leakage parameter. A more refined treatment of this term can be made
179 through unsteady models (e.g. Huayakorn et al., 1983, Kazemi et al., 1976).

180 The water flux in each phase of a medium *j* is expressed as:

$$\mathbf{j}_{lj}^{w} = \mathbf{i}_{lj}^{w} + \theta_{lj}^{w}\mathbf{q}_{lj}^{w} + \theta_{lj}^{w}S_{lj}\phi_j\dot{\mathbf{u}} = \mathbf{j}'^{w}_{lj} + \theta_{lj}^{w}S_{lj}\phi_j\dot{\mathbf{u}}; \qquad j = 1,2 \tag{7}$$

$$\mathbf{j}_{gj}^{w} = \mathbf{i}_{gj}^{w} + \theta_{gj}^{w}\mathbf{q}_{gj}^{w} + \theta_{gj}^{w}S_{gj}\phi_j\dot{\mathbf{u}} = \mathbf{j}'^{w}_{gj} + \theta_{gj}^{w}S_{gj}\phi_j\dot{\mathbf{u}}; \qquad j = 1,2 \tag{8}$$

181 where $\mathbf{i}_{lj}^{w}$ and $\mathbf{i}_{gj}^{w}$ are the non-advective fluxes of water in the liquid and gas phases; $\mathbf{j}'^{w}_{lj}$ and
182 $\mathbf{j}'^{w}_{gj}$ denote the total mass fluxes of water in the liquid and gas phases in the medium *j* with
183 respect to the solid phase that are obtained as the sum of non-advective (i.e. $\mathbf{i}_{lj}^{w}$ and $\mathbf{i}_{gj}^{w}$) and
184 advective (Dracys') fluxes (i.e. $\mathbf{q}_{lj}^{w}$ and $\mathbf{q}_{gj}^{w}$) associated with the motion of the phases in
185 each medium *j*. Equations (7) and (8) also account for the movement of the water induced
186 by the solid displacement $\dot{\mathbf{u}}$ (i.e. the water that is dragged by the soil during deformation).

187

After applying the concept of material derivative, and following an approach similar to the one described in Olivella et al. (1994), the following form of the water mass balance equations is obtained:

$$\phi_j \frac{D}{Dt}\left(\theta^w_{lj} S_{lj} + \theta^w_{gj} S_{gj}\right) + \left(\theta^w_{lj} S_{lj} + \theta^w_{gj} S_{gj}\right)\left[\left(\frac{(1-\phi)}{\rho_s}\frac{D\rho_s}{Dt}\right)^{(1-j)} + \dot{\varepsilon}_{vj}\right] + \\ +\nabla.\left(\mathbf{j}'^w_{lj} + \mathbf{j}'^w_{gj}\right) + (-1)^{j+1}\Gamma^w = f^w_j \qquad j = 1,2 \tag{9}$$

AIR MASS BALANCE EQUATION

The equations for the mass balance of air are obtained following an analogous procedure to the explained above:

$$\phi_j \frac{D}{Dt}\left(\theta^a_{lj} S_{lj} + \theta^a_{gj} S_{gj}\right) + \left(\theta^a_{lj} S_{lj} + \theta^a_{gj} S_{gj}\right)\left[\left(\frac{(1-\phi)}{\rho_s}\frac{D\rho_s}{Dt}\right)^{(1-j)} + \dot{\varepsilon}_{vj}\right] + \\ \nabla.\left(\mathbf{j}'^a_{lj} + \mathbf{j}'^a_{gj}\right) + (-1)^{j+1}\Gamma^a = f^a_j \qquad j = 1,2 \tag{10}$$

where θ^a_{lj} and θ^a_{gj} are the masses of air per unit volume of liquid and gas respectively in the medium; $\mathbf{j}^a_{lj}$ and $\mathbf{j}^a_{gj}$ denote the relative mass fluxes of air in the liquid and gas phases, with respect to the solid phase; f^a_j is the external mass supply of air per unit volume of j medium; and Γ^a is the term related to the air mass exchange between the two media. In a similar way, a quasi-steady model was also adopted for the air transfer term, as follows:

$$\Gamma^a = \gamma\left(P_{g1} - P_{g2}\right) \tag{11}$$

The air flux in each phase of the medium j is expressed as:

$$\mathbf{j}^a_{lj} = \mathbf{i}^a_{lj} + \theta^a_{lj}\mathbf{q}^a_{lj} + \theta^a_{lj}S_{lj}\phi_j\dot{\mathbf{u}} = \mathbf{j}'^a_{lj} + \theta^a_{lj}S_{lj}\phi_j\dot{\mathbf{u}}; \qquad j = 1,2 \tag{12}$$

$$\mathbf{j}^a_{gj} = \mathbf{i}^a_{gj} + \theta^a_{gj}\mathbf{q}^a_{gj} + \theta^a_{gj}S_{gj}\phi_j\dot{\mathbf{u}} = \mathbf{j}'^a_{gj} + \theta^a_{gj}S_{gj}\phi_j\dot{\mathbf{u}}; \qquad j = 1,2 \tag{13}$$

where $\mathbf{i}_{lj}^a$ and $\mathbf{i}_{gj}^a$ are the non-advective fluxes of air in the liquid and gas phases; $\mathbf{j}'_{lj}^a$ and $\mathbf{j}'_{gj}^a$ denote the total mass fluxes of air in the liquid and gas phases in the medium *j* with respect to the solid phase; which are obtained as the sum of non-advective (i.e. $\mathbf{i}_{lj}^a$ and $\mathbf{i}_{gj}^a$) and advective (Dracys') fluxes (i.e. $\mathbf{q}_{lj}^a$ and $\mathbf{q}_{gj}^a$) associated with the motion of the phases in each medium *j*. The equations (12) and (13) also account for the movement of the air induced by the solid displacement $\dot{\mathbf{u}}$ (i.e. the air that is dragged by the soil during deformation).

ENERGY BALANCE EQUATION

The balance of energy is expressed in terms of internal energy. Thermal equilibrium between phases and media is assumed. Therefore, at a given material point, the temperature is the same for all the phases and only one equation related to the total energy for the whole porous medium is required. Generally, the flow in porous media is very slow (especially in clayed soils/rocks), therefore this assumption can be considered valid in many applications. However, if the complexity of the problem (e.g. fluid injection in highly fractured rocks) justifies the necessity of a more detailed treatment of this equation, the formulation can be upgraded to consider different temperatures in the two media and phases.

Extending the approach adopted by Olivella et al. (1994) to double porosity media, the total internal energy per unit volume of porous medium was calculated by adding the internal energy of each phase in each media, as follows:

$$E = E_s \rho_s \left(1-\phi\right) + \sum_{j=1}^{2} \left(E_{lj} \rho_{lj} S_{lj} \phi_j + E_{gj} \rho_{gj} S_{gj} \phi_j \right) \qquad j = 1,2 \tag{14}$$

where E_s is the specific internal energies corresponding to the solid phase; E_{lj} and E_{gj} are the specific internal energies corresponding to the liquid and phases, respectively, of the medium j; and ρ_{lj} and ρ_{gj} are the liquid and gas phase densities. The gas phase internal energy equation adopted by Olivella et al. (1994) can be extended to double porosity media as:

$$E_{gj} \rho_{gj} = \left(E_g^w \omega_{gj}^w + E_g^a \omega_{gj}^a \right) \rho_{gj} = E_g^w \theta_{gj}^w + E_g^a \theta_{gj}^a \qquad j = 1,2 \tag{15}$$

where E^w_g and E^a_g are the specific internal energies of water and air in the gas phase, respectively; ω^w_{gj} and ω^a_{gj} are the mass fractions of water and air in the gas phase, respectively, per medium j. As in Olivella et al. (1994), this additive decomposition is also used for the liquid phase, and extended here for double porosity media:

$$E_{lj} \rho_{lj} = \left(E_l^w \omega_{lj}^w + E_g^a \omega_{lj}^a \right) \rho_{lj} = E_l^w \theta_{lj}^w + E_g^a \theta_{lj}^a \qquad j = 1,2 \tag{16}$$

where E^w_l and E^a_l are the specific internal energies of water and air in the liquid phase, respectively; ω^w_{gj} and ω^a_{gj} are the mass fractions of water and air in the liquid phase, respectively, per medium j. The specific internal energies for the individual species are (Batchelor, 1983; Pollock, 1983, and Gens and Olivella, 2001): E^w_l =4180.0 $(T\text{-}T_0)$ [J/kg]; E^w_g =2.5e^6+1900.0 $(T\text{-}T_0)$ [J/kg]; E^a_g =1006.0 $(T\text{-}T_0)$ [J/kg], and E^a_g =1006.0 $(T\text{-}T_0)$ [J/kg]. In these expressions T_0 is the reference temperature and T is [◦C]. It can be noted that the

234 specific internal energy of the vapor (i.e. water in gas phase) contains an additional term
235 that represents the latent heat in vapor. The thermal consequences of
236 evaporation/condensation are therefore taken into account in a straightforward way (Gens
237 and Olivella, 2001). As for the internal energy per unit mass of the solid phase, the law
238 suggested in the FEBEX Report (1998) was adopted in this work:

$$E_s = E_s^o T + c_p T^2 \tag{17}$$

239 where the two models parameters are: E^0_s = 732.52 [J/kg/T] and c_p =1.38 [J/kg/T^2]
240 (FEBEX Report, 1998). This law was adopted here because of the type of problems
241 presented in this paper, but it can be replaced in problems dealing with other materials.

242 Using the specific internal energies and the species mass fluxes, the energy fluxes due to the
243 motion of phases can be written as:

$$\mathbf{j}_{E_s} = E_s \rho_s (1-\phi) \dot{\mathbf{u}} \tag{18}$$

$$\mathbf{j}_{E_{lj}} = \mathbf{j}^{'w}_{lj} E^w_{lj} + \mathbf{j}^{'a}_{lj} E^a_{lj} + E_{lj} \rho_{lj} S_{lj} \phi_j \dot{\mathbf{u}} = \mathbf{j}'_{E_{lj}} + E_{lj} \rho_{lj} S_{lj} \phi_j \dot{\mathbf{u}}; \qquad j = 1,2 \tag{19}$$

$$\mathbf{j}_{E_{gj}} = \mathbf{j}^{'w}_{gj} E^w_{gj} + \mathbf{j}^{'a}_{gj} E^a_{gj} + E_{gj} \rho_{gj} S_{gj} \phi_j \dot{\mathbf{u}} = \mathbf{j}'_{E_{gj}} + E_{gj} \rho_{gj} S_{gj} \phi_j \dot{\mathbf{u}}; \qquad j = 1,2 \tag{20}$$

244 where $\mathbf{j}'_{El}$ and $\mathbf{j}'_{Eg}$ are the advective energy fluxes with respect to the solid phase.

245 Considering the hypothesis and equations discussed above, the internal energy balance
246 equation is expressed as:

$$\frac{\partial}{\partial t}\left[E_s\rho_s\left(1-\phi\right)\right]+\frac{\partial}{\partial t}\left[\sum_{j=1}^{2}\left(E_{lj}\rho_{lj}S_{lj}\phi_j+E_{gj}\rho_{gj}S_{gj}\phi_j\right)\right]+$$
$$+\nabla.\left[\mathbf{i}_c+\mathbf{j}_{Es}+\sum_{j=1}^{2}\left(\mathbf{j}_{Elj}+\mathbf{j}_{Egj}\right)\right]=\sum_{j=1}^{2}f_j^E \qquad j=1,2 \tag{21}$$

where $\mathbf{i}_c$ is the conductive heat flux; and f_j^E is the energy supply per unit volume of medium *j*.

This equation is also transformed following a similar procedure to the one explained in before for the mass balance of energy, the final form of the energy balance equation is given by:

$$\sum_{j=1}^{2}\phi_j\frac{D}{Dt}\left(E_{lj}\rho_{lj}S_{lj}+E_{gj}\rho_{gj}S_{gj}\right)+\left(1-\phi\right)\frac{D}{Dt}E_s\rho_s+$$
$$+\left(\sum_{j=1}^{2}\left(E_{lj}\rho_{lj}S_{lj}+E_{gj}\rho_{gj}S_{gj}\right)-E_s\rho_s\right)\frac{\left(1-\phi\right)}{\rho_s}\frac{D\rho_s}{Dt}+\sum_{j=1}^{2}\left(E_{lj}\rho_{lj}S_{lj}+E_{gj}\rho_{gj}S_{gj}\right)\dot{\varepsilon}_{vj}+ \tag{22}$$
$$+\nabla.\left[\mathbf{i}_c+\mathbf{j}_{Es}+\sum_{j=1}^{2}\left(\mathbf{j}_{Elj}+\mathbf{j}_{Egj}\right)\right]=\sum_{j=1}^{2}f_j^E \qquad j=1,2$$

MOMENTUM BALANCE (EQUILIBRIUM)

If inertial terms are neglected, the balance of momentum for the porous medium reduces to the equilibrium equation for total stresses:

$$\nabla.\boldsymbol{\sigma}_t+\mathbf{b}=0 \tag{23}$$

where $\mathbf{b}$ the vector of body forces, and $\boldsymbol{\sigma}_t$ is the total stress tensor (which is common for both porous media). However, effective/net stresses and fluids pressures are different for

each medium. Therefore strain-rates per each porous medium are computed. A possible decomposition of strains is:

$$\dot{\boldsymbol{\varepsilon}} = \sum_{j=1,2} \dot{\boldsymbol{\varepsilon}}_j = \sum_{j=1,2} \dot{\boldsymbol{\varepsilon}}^e_j + \dot{\boldsymbol{\varepsilon}}^p_j ; \qquad j = 1,2 \tag{24}$$

where $\dot{\boldsymbol{\varepsilon}}^e_j$ and $\dot{\boldsymbol{\varepsilon}}^p_j$ are the medium j elastic and plastic strain-rates, respectively. The total strain rate ($\dot{\boldsymbol{\varepsilon}}$) is related to solid velocities through the compatibility condition:

$$\dot{\boldsymbol{\varepsilon}} = \frac{1}{2}\left(\nabla \dot{\mathbf{u}} + \nabla \dot{\mathbf{u}}^T \right) \tag{25}$$

CONSTITUTIVE EQUATIONS

The constitutive equations establish the link between the unknowns (i.e. P_{lj}, P_{gj}, T and $\mathbf{u}$) and the dependent variables.

THERMAL CONSTITUTIVE EQUATIONS

Heat conduction is assumed to be governed by Fourier's law. As mentioned above, thermal equilibrium between phases and media was assumed, therefore the following equation can be used to calculate the conductive heat:

$$\mathbf{i}_c = -\lambda \nabla T \tag{26}$$

where λ is the global thermal conductivity of the porous medium. In this paper the global thermal conductivity proposed for the FEBEX bentonite based on the geometric mean of the thermal conductivities of the three phases was adopted (FEBEX Report, 2000):

$$\lambda = \lambda_s^{(1-\phi)} \lambda_l^{\phi S_l} \lambda_g^{\phi(1-S_l)} = \lambda_{sat}^{S_l} \lambda_{dry}^{(1-S_l)} \tag{27}$$

where λ_s, λ_l and λ_g are the thermal conductivities of the solid, liquid and gas phases, respectively; λ_{sat} and λ_{dry} are the thermal conductivities of the fully saturated and fully dry soil, respectively; they can be calculated through:

$$\lambda_{sat} = \lambda_s^{(1-\phi)} \lambda_l^{\phi}; \qquad \lambda_{dry} = \lambda_s^{(1-\phi)} \lambda_g^{\phi} \tag{28}$$

and:

$$S_l = \frac{S_{l_1} \phi_1 + S_{l_2} \phi_2}{\phi} \tag{29}$$

The thermal conductivity law can be modified/changed based on the particular materials involved in the case to be analyzed.

HYDRAULIC CONSTITUTIVE EQUATIONS

Advective fluxes of fluid phases in each medium are computed using a generalized Darcy's law:

$$\mathbf{q}_{\alpha j} = -\mathbf{K}_{\alpha j} \left(\nabla P_{\alpha j} - \rho_{\alpha j} \mathbf{g} \right) \qquad \alpha = l, g \; ; \; j = 1, 2 \tag{30}$$

where $P_{\alpha j}$ is the α phase pressure in medium j; and $\mathbf{K}_{\alpha j}$ is the permeability tensor of the α phase in medium j, evaluated as:

$$\mathbf{K}_{\alpha j} = \mathbf{k}_j \frac{k_{r\alpha j}}{\mu_{\alpha j}} \qquad \alpha = l, g \;;\; j = 1,2 \tag{31}$$

where $\mu_{\alpha j}$ is the dynamic viscosity of the α phase in the medium j; and $k_{r\alpha j}$ is the phase relative permeability of the phase α in the medium j (expressed generally as a function of the phase degree of saturation, see Eq. (33)); $\mathbf{k}_j$ is the intrinsic permeability tensor for medium j that depends on its pore structure (generally expressed through the medium porosity). Different laws are available to model this dependence, which may be selected according to the problem to be handled. For example, an exponential law (Eq. 32) was adapted to model the dependence of medium permeability on medium porosity for the compacted clay studied in the application case presented later on in this paper.

The non-advective fluxes of species inside the fluid phases, in each porous medium are computed through the Fick's law as:

$$\mathbf{i}^i_{\alpha j} = -\mathbf{D}^i_{\alpha j} \nabla \omega^i_{\alpha j} \;; \qquad i = w, a; \qquad \alpha = l, g; \quad j = 1,2 \tag{32}$$

where $\mathbf{D}^i_{\alpha j}$ is the dispersion tensor, and $\omega_{\alpha j}$ are the mass fractions (Olivella et al., 1994). Finally, the soil water retention curve (SWRC) establishes the link between the phase saturations of the medium j and the corresponding medium suction (a specific SWRC model is presented when studying the application case in a following section).

MECHANICAL CONSTITUTIVE EQUATION

A general form of the mechanical law showing (explicitly) the contributions of strains, temperature and fluid pressures is:

$$\dot{\boldsymbol{\sigma}}_j = \mathbf{D}_j \dot{\boldsymbol{\varepsilon}}_j + \mathbf{f}_j \dot{s}_j + \mathbf{t}_j \dot{T}_j ; \qquad j = 1, 2 \tag{33}$$

where $\boldsymbol{\sigma}_j$ is the constitutive stress (net or effective stress tensor), $\boldsymbol{\varepsilon}_j$ is the strain, s_j is the suction, $\mathbf{D}_j$ is the constitutive stiffness matrix, $\mathbf{f}_j$ is the generic constitutive vector relating the changes in the fluid pressures and stresses and $\mathbf{t}_j$ is the constitutive vector relating stresses and temperature (a specific mechanical model is presented in the application case).

EQUILIBRIUM RESTRICTIONS

It is assumed that the phase changes are rapid in relation to the characteristic times of the flow problem. Therefore, they can be considered in local equilibrium giving rise to a set of equilibrium restrictions that must be satisfied at all times. Equilibrium restrictions are given by the concentration of water vapor in gas phase (computed through the psychometric law), and for the concentration of dissolved air in liquid phase (evaluated by means of the Henry's law). The formulation is completed with the equations related to properties of the phases for each medium *j*.

NUMERICAL APPROACH

The equations for double porosity media quoted above were implemented in the finite element program CODE_BRIGHT. One unknown (or state variable) is associated with each one of the balance equations presented above, as follows: P_{lj} are related to the water mass balance equations (Eq. 9) for medium *j* (*j*=1,2)*;* P_{gj} are related to the air mass balance equations (Eq. 10) for medium *j* (*j*=1,2); *T* is related to the balance of internal energy equation (Eq. 22); and **U** is related to momentum balance equation (Eq. 23) The unknowns are obtained by solving simultaneously the system of PDE's (Partial Differential Equations)

numerically in a fully coupled way. From state variables, the dependent variables are calculated using the constitutive equations or the equilibrium restrictions.

The same procedure suggested in Olivella et al. (1996) was followed for the numerical treatment of the different terms of the balance equations. In summary, it can be mentioned that the numerical approach can be viewed as divided into two parts: spatial and temporal discretization. Galerkin finite element method is used for the spatial discretization while finite differences are used for the temporal discretization. The discretization in time is linear and an implicit scheme is used. Finally, since the problem presented here is non-linear, the Newton-Raphson method was adopted as iterative scheme.

Linear and quadratic interpolation functions were implemented. Analytical integration was adopted for segments, triangles and tetrahedrons. Numerical integration is used for quadrilateral, triangular prisms (6 points) and quadrilateral prisms (8 points). For the mechanical problem, selective integration was used for quadrilateral and quadrilateral prisms. Finally, for all elements the flow equations are solved using element-wise and cell-wise approximations (Olivella et al., 1996). The program has an automatic discretization of time. More details can be found elsewhere (e.g. Olivella et al., 1996; CODE_BRIGHT User's Manual, 2015).

ANALYSIS OF AN EXPANSIVE SEAL MATERIAL

In this section the hydration under confined conditions of a seal material intended for the isolation of nuclear waste is analyzed. The sample was made up of a mixture of clay-pellets and clay-powder. The pellets are generally fabricated at the factory from highly expansive clay, obtaining heavily compacted granulated materials (dry density, $\rho_d \sim 2.0$ Mg/m^3).

341 The clay-pellet mixtures have been actively studied in the context of the high level waste
342 repository design (Alonso et al., 1995, 2011; Volckaert et al., 2000; Pasquiou, 2001;
343 Hoffmann et al., 2007; Gens et al., 2011). This material exhibits the typical response of
344 expansive soils, among others: large swelling strains under wetting, high swelling pressures
345 under confinement conditions, macro-structural collapses, more than one swelling stages,
346 and irreversible behavior. These types of mixtures have a number of convenient
347 characteristics (and properties) that made them very interesting for constructing barriers
348 and seals. For example, thanks to the high-density of the clay-pellets, it is possible to
349 achieve target densities of the barrier with a low compaction effort. This is particularly
350 useful when a small and/or irregular volume needs to be sealed. Furthermore, these
351 mixtures are able to satisfy the basic properties imposed to engineered barriers and seals,
352 such as: very low permeability, mechanical stability for the waste canister, and ability to seal
353 discontinuities in the emplacement boreholes and drifts.

354 In these types of mixtures it is possible to distinguish two basic pore levels:

355 • Medium 1: corresponds to the granular skeleton of the clay mixture
356 (macrostructure). It is composed by the arrangements of the clay-pellets, the clay
357 powder (if any), and the macropores between them (Fig. 2b).

358 • Medium 2: corresponds to the high density pellets and the small pores inside them
359 (microstructure).

360 Obviously it may be possible to include more pore levels in the analysis, for example, one
361 could consider that inside the clay-pellets there are clay-aggregates, with their inter-

362 aggregate and intra-aggregate pores space. In this case three different types of pores can be
363 distinguished: i) the inter-pellets pores (i.e. the big macro pores between pellets), ii) the
364 inter-aggregates pores (i.e. pores between clay aggregates inside the pellets); and iii) the
365 intra-aggregates pores (i.e. the pores inside the clay aggregates). However, in the analysis
366 presented hereafter, only two basic structural levels were considered, and the pores types ii)
367 and iii) were associated with the microstructure. If deemed convenient, the approach can
368 always be extended to include one or more additional pores levels.

369 In order to properly handle this complex mechanical behavior the double structure (DS)
370 approach proposed originally by Gens and Alonso (1992) was adopted in this work. This
371 framework was then upgraded by (among others): Alonso et al. (1999) and Sánchez et al.
372 (2005). This last version was adopted in this work. The DS model is very appropriate for
373 analyzing this type of problem, because it explicitly contemplates the two porous media
374 identified above, as explained below.

375 **DS MECHANICAL MODEL**

376 The double structure constitutive model adopted in this work has been discussed in detail
377 in previous publications (e.g. Gens and Alonso 1992; Alonso et al., 1999; and Sánchez et
378 al., 2005, 2012). For sake of completeness, only the main model components are briefly
379 introduced as follows. The model consists of three main components: i) constitutive
380 equation for describing the behavior of the macrostructure; ii) a model for describing the
381 response of the microstructure; and iii) a law for modeling the interaction between the
382 macro and micro structures.

383 A modified Barcelona Basic Model (*BBM*) (Alonso et al., 1990) is adopted for the
384 macrostructure. The *BBM* considers two independent stress variables: the net stresses (σ),

385 computed as the excess of the total stresses over the gas pressure ($\boldsymbol{\sigma}_t$-$\mathbf{I}p_g$), and the matric
386 suction associated with medium 1 (s_1), computed as the difference between the gas and
387 liquid pressures ($s_1=p_g-p_{l1}$). The elasto-plastic *BBM* allows the extension of the modified
388 Cam-Clay model to the unsaturated condition by including a dependence of the yield
389 surface on matric suction (Fig. 3.a):

$$F_{LC} = 3J^2 - \left[\frac{g(\theta)}{g(-30^o)}\right]^2 M^2 \left(p + p_s\right)\left(p_0 - p\right) = 0 \tag{34}$$

390 where M is the slope of the critical state; p_o is the apparent unsaturated isotropic pre-
391 consolidation pressure at a specific value of suction; $g(\theta)$ is the Lode's angle function; and p_s
392 considers the dependence of shear strength on suction and temperature. When yielding
393 take places, the increment of plastic deformations is evaluated through:

$$\dot{\boldsymbol{\varepsilon}}^p_{LC} = \lambda_{LC} \frac{\partial G}{\partial \boldsymbol{\sigma}} \tag{35}$$

394 where λ_{LC} is the plastic multiplier and G is the plastic potential (Eq. (A.1), Appendix). The
395 hardening law is expressed as a rate relation between the volumetric plastic strain and the
396 saturated isotropic pre-consolidation stress 'p^*_0' (Fig. 3a)):

$$\frac{\dot{p}^*_0}{p^*_0} = \frac{(1+e)}{\left(\lambda_{(0)} - \kappa\right)} \dot{\varepsilon}^p_v \tag{36}$$

where e is the void ratio; ε_v^p is the volumetric plastic strain; κ is the elastic compression index for changes in p; and $\lambda_{(0)}$ is the stiffness parameter for changes in p for virgin states of the soil in saturated condition. The trace of the yield surface on the isotropic p-s_1 plane is called the *LC* (Loading-Collapse) yield curve and it represents the locus of activation of irreversible deformations due to loading increments or wetting collapse (Fig. 3b). More details about the *BBM* are presented in the Appendix.

It is assumed that the behavior of the high-density clay-pellets (medium 2, microstructure) is mainly volumetric and controlled by a non-linear elastic law:

$$\dot{\varepsilon}_{v2}^{e} = \frac{\dot{\hat{p}}}{K_2} \tag{37}$$

where K_2 is the bulk modulus of medium 2 (see Appendix) and $\hat{p}$ is a generalized effective stress:

$$\hat{p} = p_2 + \chi s_2 \tag{38}$$

where p_2 is the net mean stress; and s_2 is the suction related to medium 2 (i.e. p_g-p_{l2}). The framework can be extended to consider plastic behavior of the pellets as well, however in this case, and for the sake of the simplicity, a nonlinear elastic behavior was assumed.

It was assumed that χ is a constant ($\chi > 0$). Fig. 3b) shows a schematic representation of the model on the p-s plane. In these plots s is a generic suction, which can be s_1 or s_2 depending on if medium 1 or 2 is analyzed, respectively. In the p-s_2 plane the line corresponding to constant $\hat{p}$ is referred to as Neutral Line (F_{NL}), since no microstructural deformation occurs when the stress path moves on it.

415 The interaction between the two pore levels is considered by assuming that elastic volume
416 changes of the pellets (microstructure) may modify the global arrangement of the material
417 (macrostructure) in an irreversible manner (e.g. Gens and Alonso, 1992). The associated
418 plastic irreversible deformations are computed according to:

$$\dot{\varepsilon}_{v\ 1\to 2}^{p} = f\,\dot{\varepsilon}_{v\ 2}^{e} \tag{39}$$

419 where f is an interaction function that depends on the degree of openness of the
420 macrostructure through the ratio p/p_o (e.g. Gens and Alonso, 1992).

421 The total plastic macrostructural strain $\left(\dot{\varepsilon}_{v}^{p}\right)$ used in Eq. (36) is obtained as:

$$\dot{\varepsilon}_{v}^{p} = \dot{\varepsilon}_{v\ LC}^{p} + \dot{\varepsilon}_{v\ 1\to 2}^{p} \tag{40}$$

422 The coupling between macro and micro levels is given by p_o^* (the hardening variable of the
423 macrostructure, Fig. 3a), which depends on the total plastic volumetric strain (36). In this
424 way it is considered that the microstructural changes can affect the global arrangements of
425 clay aggregates. More details can be found elsewhere (e.g. Alonso 1998; Sánchez et al.,
426 2005).

427 **HYDRAULIC MODEL**

428 Darcy's generalized law (Eq. 30) rules the unsaturated flow in the two porous media. Note
429 that both porous media contain interconnect porosity and the flow will depend basically on
430 the permeability of each media and the corresponding gradient of pressures. The saturated
431 permeability of expansive clays shows a strong dependence on porosity. Fig. 4a) shows

experimental data related to the Serrata clay, also known as FEBEX bentonite (Volckaert et al. 2000; and Huertas et al., 2006). The following exponential law was adapted to model the dependence of permeability on medium porosity:

$$\mathbf{k}_j = \mathbf{k}_o \exp\left(b\left(\phi_j - \phi_o\right)\right) \qquad j = 1,2 \tag{41}$$

where $\mathbf{k}_0$ is the reference permeability tensor at the reference porosity ϕ_0, and b is a model parameter. It should be noted that both media have the same parameters with the only difference being the value of the actual (medium) porosity.

The well-known cubic law was adopted for the relative permeability model:

$$k_{rl\ j} = S_{l\ j}^3 \qquad j = 1,2 \tag{42}$$

A SWRC based on a modified van Genuchten model was adopted in this study:

$$S_{l\ j} = f_d \left[1 + \left(\frac{s_j}{P_o}\right)^{\frac{1}{1-\lambda_o}}\right]^{-\lambda_o} \text{; with} \qquad f_d = \left(1 - \frac{s_j}{P_d}\right)^{\lambda_d} \qquad j = 1,2 \tag{43}$$

where P_o and λ_o are models parameter. The function f_d is included to improve the model prediction at high suctions, P_d being a parameter related to the suction when $S_l \sim 0$ (P_d being ~1100 MPa), and λ_d is a model parameter. When $\lambda_d = 0$ the original van Genuchten (1980) model is recovered. Fig. 4b) presents tests results for FEBEX bentonite alongside the adopted SWRC models. Finally, it was assumed that the gas pressure in both media is the same (and equal to the atmospheric pressure). In this case only one mass transfer term (i.e. for water) was considered.

MODELING

This section presents the analysis of the test coded as 'Reseal16' by Volckaert et al. (2000). The sample was made up from Serrata clay by mixing (in weight) 50% of clay-pellets and 50% of clay-powder, achieving a global density of 1.55 Mg/m^3. The dry density of the pellets was 2.05 Mg/m^3 and Gs=2.70. The test was carried out in a cell with hydration from both ends in a cylindrical sample 5 cm high and 12cm diameter. The experimental data generated in the context of the Reseal project (Volckaert et al. 2000) and FEBEX projects (Huertas et al., 2006), was used to identify the main model parameters. The parameters related to the water retention curves and permeability law were obtained independently from single elements tests performed on compacted samples prepared at different densities. The experimental data was presented in Figures 4a) and 4b). As for the DS model, the BBM parameters κ_o, κ_s, $\lambda_{(0)}$, ζ, r, P^*_o, were adopted from independent tests performed in Serrata clay and suggested values reported in Volckaert et al. (2000). The elastic parameters of the microstructure are equal to ones of the elastic part of the BBM. The parameters related to the interaction functions were obtained from model calibration. An initial relative humidity close to 22 % was measured (Volckaert et al. 2000), and therefore an initial suction of 210 MPa was adopted for both media. According to the SWRC the initial saturation in medium 2 (clay-pellets) is $S_{l2} = 0.59$. This implies an initial water content of the clay-pellets~6.9%, which is very close to the reported one (~6.4 %). As for medium 1, the initial $S_{l1} = 0.06$. Based on the experimental data, the following macro and micro porosity values were adopted: $\phi_1 = 0.335$, and $\phi_2 = 0.097$. The test was simulated as a 1-D boundary value problem. Tables 1 and 2 list the parameters related to the mechanical and flow problems, respectively.

Fig. 5a) presents the comparisons between experimental (symbols) and model (line) results. This test (as all the other tests reported by Volckaert et al. (2000)) showed two swelling steps, with the three main stages: i) an initial stage, related to a (quite fast) swelling; ii) a transition stage, with a moderate swelling; and iii) a second and final swelling. The model was able to reproduce this behavior by distinguishing each swelling phase according to the structural level involved in it. The first swelling is ascribed to the medium 1. The water flowing through the (big) interconnected macropores hydrated first the periphery of the clay-pellets and the clay-powder, inducing an initial expansion of the sample. This swelling tends to close the macropores and also to induce an increase of the swelling pressure (stage 1). Once the more accessible clay minerals were hydrated, the rate of swelling decreases (stage 2). This stage is related to the delayed transfer of water from the macro level (1), to the clay-pellet (intraaggregate) level (2). This stage is mainly control by the leakage term (Eq. 20). Then, the swelling rate increased again (third stage), induced by the delayed hydration (and associated swelling) of the high-density clay-pellets. The model results in terms of water intake are also quite satisfactory. Fig. 5b) shows the time evolution of the two media porosities (scaled respect their initial porosities) for a point located at the center of the sample. It is observed that the macroporosity tends to increase at the beginning of the hydration (i.e. around between 1 and 3 days) because of the initial hydration quoted above, but decrease substantially afterwards when the microstructure swells.

Fig. 5c) presents the time evolution of the suctions (associated with each porous media) at two different positions: i) a point located at the hydration boundary (identify as 'sup'), ii) a point at the center of the specimen (coded as 'cent'). Initially the water flow took place predominantly through the macropores (medium 1) by advection. At the same time water

493 was slowly transferred from the macropores to the clay-pellets (medium 2), via the leakage
494 term, leading to an equilibration of both suctions in the long term.

495 Fig. 6a) presents the evolution of the intrinsic permeability of each medium in a zone close
496 to the hydration boundary. Initially, there was a significant permeability contrast between
497 the two porous media, which implies that the macropores acted as preferential path-ways.
498 However, as the pellets were hydrated (through water mass transfer term between media)
499 they expanded and compressed the macropores, leading to a more homogeneous material
500 at the end of the test, with similar permeability values in both media. According to Fig. 6b),
501 the model predicts that this homogenization took place in zones close to hydration front
502 mainly, because in zones away from it (i.e. near the center of the sample) the two different
503 pore levels still remained. This result is in agreement with the observations of the
504 postmortem test of this sample reported by Volckaert et al. (2000).

505 It has been shown that proposed double porosity formulation was able to reproduce the
506 main relevant physical phenomena observed in this test involving a clay mixture.

507 ## ANALYSIS OF CELL INFILTRATION TESTS

508 The behavior of the unsaturated compacted FEBEX bentonite during infiltration cell tests
509 is studied in this section under thermal gradient and isothermal conditions. The next
510 section focuses on the material and the results from the swelling pressure tests. Afterwards,
511 the infiltration tests are presented together with the associated modeling.

MATERIAL AND SWELLING PRESSURE TESTS

The FEBEX bentonite was selected by ENRESA (Spanish Agency for Radioactive Waste Management) for backfilling and sealing functions in nuclear waste repositories. The montmorillonite content of this clay is higher than 90%. Its liquid and plastic limits are 102% and 53%, respectively. The relatively low values of the Atterberg's limits can be attributed to the significant quantity of 'silt-sized aggregates', which are pseudomorphs of the volcanic minerals transformed into smectite (Villar, 2002). Fig. 7a) shows the (granulated) raw material used in the experiments. Fig. 7b) shows the uniaxially and statically compacted samples in the oedometer ring used to determine the swelling pressure of this material. The inner diameter and length of the specimens were 5.0 and 1.2 cm respectively. Nominal dry densities (ρ_d) varying between 1.40 and 1.70 Mg/m^3 were obtained by this method.

Fig. 7c) shows the clear bimodal pore size distribution observed from mercury intrusion porosimetry (MIP) tests performed on two samples of FEBEX bentonite compacted at two different ρ_d: 1.5 Mg/m^3 and 1.8 Mg/m^3. The dominant pore size around 10 nm corresponds to the pores inside clay aggregates (i.e. small 'intra-aggregate'). The larger pore size depends on the dry density and ranges from 10 μm (for ρ_d=1.8 Mg/m^3) to 40 μm (for ρ_d=1.5 Mg/m^3). These larger voids would correspond to the 'inter-aggregate' pores. This double structure was also detected using other techniques, such as Scanning Electron Microscope and water retention curve tests (Lloret et al., 2003). The two dominant pore sizes could be associated with two basic structural levels (Fig. 2b)): i) the macrostructure, related to the global arrangements of clay aggregates (with macropores between them); and ii) the microstructure, which corresponds to the active clay minerals (with micropores inside the clay aggregates).

536 The samples were hydrated at constant volume through the bottom surface with deionized
537 water injected at a pressure of 0.6 MPa, while the upper outlet remained open to
538 atmosphere. At the same time, the load cell measured the swelling pressure exerted by the
539 clay. The small vertical deformations of the specimen, arising mainly from the load cell and
540 frame deformability, were measured by LVDTs. The actual density after the tests differed
541 slightly from the nominal one due to the small displacement allowed by the equipment (e.g.
542 about 0.4 mm when the vertical stress was 7 MPa). The tests were performed at a constant
543 temperature of around 27±2°C. Fig. 8a) shows a photo of the high pressure oedometer,
544 while Fig. 8b) presents a scheme of the apparatus indicating its main components. The
545 FEBEX bentonite has been extensively investigated during the last few years and detailed
546 information about this material can be found elsewhere (e.g. Villar, 2002; Huertas et al.,
547 2006; Lloret et al.; 2003; Gens et al., 2009).

548 Typical results of the swelling-pressure tests are presented in Fig. 9. Swelling pressure
549 started to increase as soon as the water was in contact with the clay, but it did not develop
550 at a constant rate. After a sharp initial increase, there was a period of time in which the
551 pressure increased more slowly (or even remained fairly constant for some hours), and then
552 increased again, in a second and final swelling period. This behavior is more apparent in
553 samples of lower ρ_d.

554 These tests were simulated as a boundary value problem using a 1-D model. The same
555 constitutive laws presented in the previous section were used in the simulations. Table 3
556 contains the main parameters adopted in the modelling. According to Gens and Alonso
557 (1992), the dependence of swelling pressure on initial density can be taken into account

558 through p_0^*. Three stages were detected in the tests: i) an initial swelling, that can be
559 associated with the hydration and swelling of the more accessible clay minerals., ii) a
560 transition stage between the first and the second swelling; and iii) a final swelling
561 corresponding to the eventual hydration of the clays aggregates (i.e. the 'silt-sized
562 aggregates' mentioned above), modeled in this framework through the microstructural law
563 (Eq. 28). The transition stage is related to the water transfer from the macro to micro
564 structure. In low density (high-porosity) samples, the flow and hydration through the
565 macropores took place very fast, when compared against the time needed for the hydration
566 (and swelling) of the clay aggregates. Because of this, there is a clear differentiation between
567 the first and second swellings. In denser (low permeability) samples, the two characteristic
568 times (i.e. flow through the macropores and aggregates hydration) are similar, and this is
569 why there is not a marked difference between the first and second swellings. This aspect is
570 properly controlled through the leakage term used in this formulation. It can be seen that
571 the model is able to reproduce quite satisfactorily the three observed stages, both in terms
572 of kinetics of swelling and also maximum swelling pressure values.

573 **INFILTRATION TESTS**

574 Two infiltration tests were performed by CIEMAT (Spain) in cylindrical cells 40 cm long
575 and 7 cm diameter. They were made of Teflon© to minimize lateral heat conduction, and
576 were externally covered with steel semi-cylindrical pieces to prevent the deformation of the
577 cell by bentonite swelling. In one of the tests (GT40) the clay was heated through the
578 bottom surface at a constant temperature of 100ºC. The other test (IT40) was carried out at
579 isothermal conditions. The cells were instrumented with relative humidity and temperature
580 sensors placed inside the clay at three different levels separated by 10 cm. The relative
581 humidity and temperature evolution at different levels inside the clay were recorded. The

582 FEBEX clay was compacted with its hygroscopic water content (around 14 %) at an initial
583 nominal dry density of 1.67 Mg/m^3. Granitic water was injected through the upper part of
584 the cells (in both tests) at a pressure of 1.2 MPa. Fig. 10a) shows a photo of the cells during
585 operation, while Fig. 10b) illustrates the experimental setup showing its main components.
586 More details can be found in Villar and Gómez-Espina (2009).

587 The tests were modeled with two different *THM* approaches: i) a single porosity model,
588 using an equivalent porosity, and ii) a double porosity model that distinguishes the two
589 basic pore levels present in this material (i.e. Fig. 7c). As for i), the model known as
590 Operational Base Case (OBC) was adopted in this study. The OBC model was used in a
591 number of simulations related to other FEBEX experiments, and it can be considered as a
592 'standard' approach to analyze this type of problem. The OBC has been extensively
593 reported in the literature (e.g. Villar et al., 2008; Gens et al., 2009, Sánchez et al., 2012.a,
594 2012.b). The main constitutive laws and model parameters of the OBC model are
595 presented in Table 4. As for the double porosity/structure model (coded as 'DS'), the same
596 constitutive equations presented in the previous sections were adopted in this analysis.

597 Fig. 11a) presents the results in terms of relative humidity for the cell IT40; Fig 11b) shows
598 similar results for the cell GT40; and Fig 11c) presents the time evolution of temperature
599 for test GT40. In these three plots the experimental data is represented with symbols, the
600 OBC results with dash lines, and the DS outputs with solid lines. All the results are
601 presented for a period of 10 years. As for the relative humidity, it can be seen that the OBC
602 model predict a relatively quick saturation of the clay, faster than the experimental values in
603 both cells. A similar trend was observed in the 'mock-up test', which is a large clay-barrier
604 heating test that is being carried out at CIEMAT facilities in the context of the FEBEX

project (e.g. Sánchez et al., 2012.a). The results from the DS model are quite close to the actual observations for all the positions analyzed and for both cells. As for the evolution of temperature, both models reproduce quite well the thermal field in the GT40 cell. The OBC model tends to predict higher temperatures, particularly at advanced stages of the test. This is because of the higher saturation predicted by this model and the associated higher thermal conductivities impacting in the predicted thermal field.

In this type of clay, the water flow takes place through the macropores mainly. During clay hydration the stiffer clay-aggregates tend to expand and to close the soft-macropores (this is particularly critical under confined conditions); which lead to a reduction of the permeability associated with the macropores. The swelling of the microstructure is also associated with an increase of the microporosity and permeability related to this pore structure. However, the water at the microstructural level is strongly attached to the clay minerals. Therefore this water does not move easily under pressure gradients. For example, some works have reported that density of the absorbed water can be around 1.38 Mg/m^3 (Skipper et al., 1991), and the water viscosity can be higher up to a factor of seven (Ichikawa et al., 2002). This implies that the water mobility through the micropores is very limited. This clay-water behavior (i.e. high water density and viscosity) implies that the coefficient of permeability of the microstructure is around one order of magnitude smaller than the one of the macrostructure. The final outcome of these two phenomena (i.e. reduction of macroporosity induced by the expansion of the stiff-clay-aggregates and the limited mobility of the microstructural water) is that during wetting the pore structure of the bentonite evolve, affecting the kinetic of hydration and leading to a global decrease of the soil permeability.

628 Figures 12 presents the variation of the pore spaces during hydration in terms of void
629 ratios for the test GT. Fig. 12a) presents the distribution of global void ratio (i.e.
630 $e = \frac{v_v}{v_s} = e_1 + e_2 = \frac{v_{v1} + v_{v2}}{v_s}$) at different times. As expected, the model predicts higher void
631 ratios near the hydration front due to clay swelling; and shrinkage near the heater. Fig 12b)
632 shows that he micro-porosity tend to increase during hydration due to the wetting and
633 swelling of the active clay minerals (which are associated with the microstructural level in
634 this model). This microstructural expansion under confined conditions, tend to compress
635 the macropores (Fig 12c)) and therefore, to reduce the clay permeability, delaying the
636 hydration process. It can be observed that the double porosity model in conjunction to the
637 double structure mechanical law plays an instrumental role in properly predicting the clay
638 barrier behavior.

639 ## CONCLUSIONS AND REMARKS

640 In many engineering problems the use of a double porosity formulation is more realistic
641 because it is possible to take explicitly into account the different phenomena that take place
642 in each void level, with their respective constitutive laws, parameters and also their mutual
643 interactions. In this work a fully coupled *THM* formulation for dual porosity materials was
644 proposed. The formulation is very general and able to incorporate different constitutive
645 laws for the mechanical, hydraulic and thermal problem for each pore level considered. The
646 formulation was implemented in the finite element program CODE_BRIGHT and it was
647 used with success to solve problems related to double structure media, involving
648 heterogonous man-made soils made up from high-density clay-pellets mixtures, and also
649 compacted expansive soils.

It was observed that the double porosity framework was able to capture features of soil behavior that is not possible to reproduce with single porosity approaches. In particular, the double porosity model was capable to simulate the presence of more than one swelling stages in expansive materials, and explain the kinetic of swelling observed in samples prepared at different dry densities. It was also able to model the slow rate of hydration observed in infiltration tests. Experiments at constant temperature and with thermal gradient were analyzed. Thanks to the explicit inclusion of the two pore levels (very characteristic of expansive clays) in the analysis, the model was able to simulate the expansion of clay minerals under confined conditions, with the consequent reduction of macroporosity and its effect on permeability.

REFERENCES

Aifantis, E. (1980). "On the problem of diffusion in solids". *Actha Mechanica,* **37**(3-4), 265-296

Alonso, E.E. (1998). "Modelling expansive soil behaviour". *Second International Conference on Unsatured Soils. Beijing, China*; **1**, 37-70.

Alonso, E.E., Gens, A, and Josa A. (1990). "A constitutive model for partially saturated soils". *Géotechnique,* **40**(3), 405-430.

Alonso, E.E., Gens, A, and Lloret A. (1991). "Double structure model for the prediction of long-term movements in expansive materials". *Computer Methods and Advances in Geomechanics (Beer, Booker, Carter, ed.) Balkema, Rotterdam*, 1, 541-548

Alonso, E.E., Lloret, A., Gens, A., and Yang, DQ. (1995). "Experimental behaviour of highly expansive double-structure clay". *Proc. 1rd Int. Conference on Unsaturated Soils, Paris. Balkema*, 1, 11-16.

Alonso, E. E., Olivella, S., and Pinyol, N. M. (2005). "A review of Beliche Dam". *Géotechnique* 55(4), 267–285

Alonso, EE. Romero, E. and Hoffmann, C. (2011). "Hydromechanical behaviour of compacted granular expansive mixtures: experimental and constitutive study". *Geotechnique* 61(4), 329–344

Alonso, E.E., Vaunat, J., and Gens, A. (1999). "Modelling the mechanical behaviour of expansive clays". *Engineering Geology,* 54, 173-183.

Bai, M., Ma, Q., and Roegiers, J. (1994). "Dual-porosity behaviour of naturally fractured reservoirs". *Int. Jnl. Numer. Anal. Meth. Geomech.*, 18, 359- 376.

Barrenbaltt, G., Zeltov, I., and Kochina, N. (1960). "Basic concepts in the theory of seepage of homogeneous liquids in fissured rocks". *Pirkl. Mat. Mekh.*, 24, 852-864

Batchelor, G:K: (1983). "Fluid Dynamics". *Cambridge University Press.*

Birkholzer, J., and Tsang, W. (2000). "Modelling the thermal-hydrologic processes in a large-scale underground heater test in partially saturated fractured tuff". *Water Resources Research,* 36(6), 1431-1447.

Borja, R., and Koliji A. (2009). "On the effective stress in unsaturated porous continua with double porosity". *Journal of the Mechanics and Physics of Solids,* 57, 1182–1193

Callari, C., and Federico, F. (2000). "FEM validation of a double-porosity elastic model for consolidation of structurally complex clayey soils". *Int. Jnl. Numer. Anal. Meth. Geomech.*, 24, 367- 402.

Carrera, J., Sánchez-Vila, X., Benet I, Medina A, Galarza G, and Guimerà J. (1997). "On matrix diffusions: formulations, solution methods and qualitative effects". *Hydrogeology Journal,* 6, 178-190.

Ellsworth, D., and Bai, M. (1992). "Flow-Deformation Response of Dual-Porosity Media". *Journal of Geotechnical Engineering*, 118(1), 107-124.

Gens, A., Alonso, E.E. (1992). "A framework for the behaviour of unsaturated expansive clays". *Can. Geotech. Jnl.*, 29, 1013-1032.

Gens, A., Garcia Molina, A, Olivella, S., Alonso, E.E. and Huertas, F. (1998). "Analysis of a full scale in-situ test simulating repository conditions". *Int. Jnl. Numer. Anal. Meth. Geomech*, 22, 515- 548.

Gens, A., Sánchez, M., Guimaraes, L., Alonso, E.E., Lloret, A., Olivella, S., Villar, M.V., and Huertas, F. (2009). "A full scale in situ heating test for high level nuclear waste disposal. Observations, analysis and interpretation". *Géotechnique*, 59, 377-399.

Gens, A., Vallejan, B., Sánchez, M., Imbert, C., Villar, MV., and Van Geet, M. (2011). "Hydromechanical behaviour of a heterogeneous compacted soil: experimental observations and modeling". *Géotechnique*, 61(5), 367 –386.

Ghafouri, H. and Lewis, R. (1996). "A finite element double porosity model for heterogeneous deformable porous media". *Int. Jnl. Numer. Anal. Meth. Geomech.,* 20, 831-844.

Hoffmann, C., Romero, E, and Alonso, EE. (2007). "Hydro-mechanical behaviour of bentonite pellet mixtures". *Physics and Chemistry of the Earth* 32: 832–849

Hueckel, T. (1992). "Water-mineral interaction in hygromechanics of clays exposed to environmental loads: a mixture-theory approach". Can. Geotech. J. 29: 1071-1086

Huertas, F., Farina, P., Farias, J., Garcia-Sineriz, J.L., Villar, M.V., Fernandez, A.M., Martin, P.L., Elorza, F.J., Gens, A., Sánchez, M., Lloret, A., Samper, J., and Martinez, M.A. (2006). "Full-scale engineered barrier experiment. Updated Final Report". *Technical Publication 05-0*/2006, ENRESA, Madrid.

Huyakorn, B., Lester, A., and Faust C. (1983). "Finite element techniques for modelling groundwater flow in fractured aquifers". *Water Resources Research*, 19(4), 1019-1035.

Kazemi, H., Merril, L., Porterfield, K. & Zeman, P. (1976). "Numerical simulation of water-oil flow in naturally fracturated reservoirs". *Soc. Pet. Eng. Jnl.* 16, 317-326

Khalili, N., and Selvadurai, A.P (2003). "A fully coupled constitutive model for thermo-hydro-mechanical analysis in elastic media with double porosity". *Geophys. Res. Lett.*, 30(24), 2268.

Khalili, N., Valliappan, S., and Wan, C. (1999). "Consolidation of fissured clays". *Géotechnique*, 49 (1), 75-89.

Lewis, R., and Ghafouri, H. (1997). "A novel finite element double porosity model for multiphase flow through deformable fractured porous media". *Int. Jnl. Numer. Anal. Meth. Geomech,* 21, 789-816.

Lloret, A., Villar, M.V., Sánchez, M., Gens, A., Pintado, X., and Alonso, E. (2003). "Mechanical behaviour of heavily compacted bentonite under high suction changes". *Géotechnique*, 53(1), 27-40.

Mašín, D. (2013). "Double structure hydromechanical coupling formalism and a model for unsaturated expansive clays". *Engineering Geology*; 165(24), 73–88

Master, I., Pao, W., and Lewis, R. (2000). "Coupling temperature to a double-porosity model of deformable porous media. *Int. J. Numer. Meth. Engng*; 49, 421-438.

Musso, A., and Federico, F. (1993). "Consolidation of highly fissured clays" (in Italian). *Rivista Italiana di Geotecnia*; 3, 247-273.

Olivella, S., Carrera, J., Gens, A., and Alonso E.E. (1994). "Non-isothermal multiphase flow of brine and gas through saline media". *Transport in porous media*, 15, 271-293.

744 Olivella, S., Gens, A., Carrera, J. and Alonso EE. (1996). "Numerical formulation for a
745 simulator (CODE-BRIGHT) for the coupled analysis of saline media". *Engineering*
746 *Computations,* 13(7), 87-112.
747 Pasquiou, A. (2001). "Pellets d'argile gonflante elaboration et caracterisation
748 hydromecanique". *Phd Thesis* L' Université des Sciences et Technologie de Lille, France.
749 Pollock, D.W. (1986). "Simulation of fluid flow and energy transport processes associated
750 with high-level radioactive waste disposal in unsaturated alluvium". *Water resource research,* 22
751 (5), 765-775.
752 Sánchez, M. (2004). "Thermo-Hydro-Mechanical coupled analyses in low permeability
753 media". *PhD Thesis, Universitat Politècnica de Catalunya, Spain*. 2004
754 Sánchez, M., Gens, A., Guimaraes, L., and Olivella, S. (2005). "A double structure
755 generalized plasticity model for expansive materials". *Int. Jnl. Numer. Anal. Meth. Geomech,*
756 29, 751–787
757 Sánchez, M., Gens, A., and Olivella, S. (2012.a). "THM Analysis of a large scale heating test
758 incorporating material fabric changes". *Int. Jnl. Numer. Anal. Meth. Geomech,* 36(4), 391-421.
759 Sánchez, M., Gens, A., and Guimarães L. (2012.b). "Thermal–hydraulic–mechanical
760 (THM) behaviour of a large-scale in situ heating experiment during cooling and
761 dismantling". *Canadian Geotechnical Journal,* 49(10),1169-1195.
762 van Genuchten M.Th. (1980). "A closed-form equation for predicting the hydraulic
763 conductivity of unsaturated soils". *Soil Science Society of America Journal*, 44(5), 892–898.
764 Villar, M.V., 2002. "Thermo-hydro-mechanical characterisation of a bentonite from Cabo
765 de Gata. A Study Applied to the Use of Bentonite as Sealing Material in High Level
766 Radioactive Waste Repositories". *Publicación Técnica ENRESA* 01/2002. Madrid. 258 pp.
767 Villar, M.V., and Gómez-Espina, R. (2009). "Report on thermo-hydro-mechanical
768 laboratory tests performed by CIEMAT on FEBEX bentonite 2004-2008". *CIEMAT*,
769 Madrid
770 Villar, M.V., Sánchez, M., AND Gens., a. (2008). "Behaviour of a bentonite barrier in the
771 laboratory: Experimental results up to 8 years and numerical simulation". *Physics and*
772 *Chemistry of the Earth,* 33, S476–S485.
773 Volckaert, G., Dereeper, B., Put, M., Ortiz, L., Gens, A., Vaunat, J., Villar, MV., Martin,
774 P.L., Imbert, C., Lassabatère, T., Mouche, E., and Cany, F. (200). "A large-scale in situ
775 demonstration test for repository sealing in an argillaceous host rock". *Reseal project - Phase I.*
776 *EUR 19612 EN,* European Commission, Brussels.
777 Warren, J., and Root, P (1963). "The behaviour of naturally fracturated reservoirs". *Trans*
778 *AIME*, 22(8), 245-255.
779 Wilson, R., and Aifantis, E. (1982). "On the theory of consolidation with double porosity".
780 *Int. J. Engng Sci.*, 20 (9), 1019-1035.
781

APPENDIX

The *BBM* model is adopted to describe the behavior of medium 1, also identified as macrostructure. The corresponding yield surface (F_{LC}) is given by (25) and the plastic potential (G) is expressed as:

$$G = \alpha_G 3J^2 - \left[\frac{g(\theta)}{g(-30°)}\right]^2 M^2 (p + p_s)(p_0 - p) = 0 \tag{A1}$$

where α_G is determined according to (Alonso et al., 1990) . The dependence of the tensile strength on suction and temperature is given by:

$$p_s = k s_1 e^{-\rho \Delta T} \tag{A2}$$

where k and ρ are model parameters. The dependence of p_0 on suction is given by:

$$\text{(a) } p_0 = p_c \left(\frac{p_{0T}^*}{p_c}\right)^{\frac{\lambda_{(0)} - \kappa}{\lambda_{(s)} - \kappa}} ; \qquad \text{b) } p_{0T}^* = p_0^* + 2\left(\alpha_1 \Delta T + \alpha_3 \Delta T |\Delta T|\right) \tag{A3}$$

where p_c is a reference stress, α_1 and α_3 are models parameters. $\lambda_{(s)}$ is the compressibility parameter for changes in net mean stress for virgin states of the soil. This parameter depends on suction according to:

$$\lambda_{(s)} = \lambda_{(0)} \left[r + (1 - r)\exp(-\zeta s_1)\right] \tag{A4}$$

where r is a parameter which defines the minimum soil compressibility (at infinite suction) and ζ is a parameter which controls the rate of decrease of soil compressibility with suction. The macrostructural bulk modulus (K) for changes in mean stress is evaluated with the following law:

800 $$K_1 = \frac{(1+e)}{\kappa} p \qquad \text{(A5)}$$

801 where κ is evaluated according to.

802 $$\kappa = \kappa_i \left(1 + \alpha_s s_1\right) \qquad \text{(A6)}$$

803 The macrostructural bulk modulus for changes in suction is computed considering the
804 following law:

805 $$K_s = \frac{(1+e_1)(s_1 + p_{atm})}{\kappa_s} \qquad \text{(A7)}$$

806 where κ_s is evaluated according to.

807 $$\kappa_s = \kappa_{s0}\left(1 + \alpha_{sp} \ln p / p_{ref}\right) \qquad \text{(A8)}$$

808 The microstructural bulk modulus (K_2) can be calculated according to the two possible
809 equations as follows, depending on the microstructural model adopted (Sánchez, 2004):

810 $$\text{a) } K_2 = \frac{e^{-\alpha_m \hat{p}}}{\beta_m} : \qquad \text{b) } K_2 = \frac{\left(1+\bar{e}_2\right)}{\kappa_2}\hat{p} \qquad \text{(A9)}$$

811 where α_m and β_m are model parameters for the exponential model A9a), and κ_2 is a model
812 parameter for the model A9b).

813 The global bulk modulus can be calculated as follows:

814 $$K = \left(\frac{1}{K_1} + \frac{1}{K_2}\right)^{-1} \qquad \text{(A10)}$$

815 The shear modulus is calculated through:

816 $$G_T = \frac{3(1-2\mu)K}{2(1+\mu)} \quad \text{(A11)}$$

817 The macrostructural bulk modulus for changes in temperature is computed considering the
818 following law:

819 $$K_T = \frac{1}{(\alpha_0 + \alpha_2 \Delta T)} \quad \text{(A12)}$$

820 where α_0 and α_2 are parameters related to the elastic thermal strain.

Notation

α	phase index, *s* solid, *l* liquid, *g* gas.	F_{NL}	Neutral Line
α_G	parameter related to the plastic potential	f	interaction function between structural levels
α_0	parameter for elastic thermal strain	f^i_j	external mass supply per unit volume of medium (i=*w,a,*; j=1,2)
α_1	parameter that relates p_o^* with T	f^{E_j}	Internal/external energy supply per unit volume of medium (j=1,2)
α_2	parameter for elastic thermal strain	$\mathbf{g}$	gravity vector
α_3	parameter that relates p_o^* with T	G	plastic potential
α_m	parameter controlling the microstructural soil stiffness	G_t	shear modulus
α_s	parameter related to the soil stiffness	g	lode angle function
χ	F_{NL} slope	$\mathbf{I}$	identity matrix
ΔT	temperature increment (T- T_0)	$\mathbf{i}^i_{\alpha j}$	non-advective mass flux (i=*w,a;* α=*l,g;* j=1,2)
$\boldsymbol{\varepsilon}$	strain vector. $\{\varepsilon_x,\varepsilon_y,\varepsilon_z,\gamma_{xy},\gamma_{xz},\gamma_{yz}\}^T$	$\mathbf{i}_{cj}$	non-advective heat flux (j=1,2)
$\dot{\boldsymbol{\varepsilon}}^e$	elastic strain increment due to stress changes	J	2nd stress invariant of deviatoric stress tensor
$\dot{\boldsymbol{\varepsilon}}^p$	plastic strain increment due to stress changes	$\mathbf{j}^i{}_{Ej}$	advective energy flux in α–phase with respect to a fixed reference system (j=1,2)
ε^p_{v1}	plastic volumetric strain of medium 1	$\mathbf{j}'^i{}_{Ej}$	advective energy flux in α–phase with respect to the solid phase (j=1,2)
ε^p_{v2}	plastic volumetric strain of medium 2	$\mathbf{j}^i{}_{\alpha j}$	total mass flux of *i*-species in α–phase with respect to a fixed reference system (j=1,2)
$\boldsymbol{\gamma}_{sj}$	elasto-plastic vector associated with suction j (j=1,2)	$\mathbf{j}'^i{}_{\alpha j}$	total mass flux of *i*-species in α–phase with respect to the solid phase (j=1,2)
$\boldsymbol{\gamma}_T$	elasto-plastic vector associated with temperature	$\mathbf{K}_{\alpha j}$	permeability tensor (α=*l,g;* j=1,2)
Γ^i	mass exchange term (i=*w,a*)	$\mathbf{k}_j$	intrinsic permeability tensor (j=1,2)
γ	leakage parameter	$k_{r\alpha j}$	α–phase relative permeability (α=*l,g;* j=1,2)
ϕ, ϕ_j	porosity , medium porosity (j=1,2)	K	global bulk modulus
ϕ_0	reference porosity	K_s	bulk modulus for changes in suction (medium 1)
κ_0	saturated elastic stiffness parameter for changes in stress	K_T	bulk modulus for changes in temperature
κ	elastic stiffness parameter for changes in stress at current suction	K_j	bulk modulus for changes in mean stress for medium j (j=1,2)
κ_s	macrostructural elastic stiffness parameter for changes in suction	k	parameter describing the increase in cohesion with suction
λ	global thermal conductivity	LC	Loading-Collapse yield surface (*BBM*)

λ_α	thermal conductivity of the α phase (α=s, l, g)	*lc*	plastic mechanism related to *BBM*
λ_{sat}	thermal conductivities of the fully saturated soil	**m**	auxiliary unit vector $\mathbf{m}^T = (1,1,1,0,0,0)$
λ_{dry}	thermal conductivities of the fully dry soil	*M*	slope of critical state line
$\lambda_{(s1)}$	macrostructural stiffness parameter for changes in net mean stress for virgin states of soil at suction s_1	$P_{\alpha j}$	fluid pressure of the α–phase (α=*l,g;* *j*=1,2)
λ_o, λ_d	retention curve parameters	P_o, P_d	retention curve parameters
μ	Poisson's coefficient	$\hat{p}$	generalized effective stress of medium2
$\mu_{\alpha j}$	dynamic viscosity of α–phase (α=*l,g;* *j*=1,2)	*p*	mean net stress
θ	Lode's angle	p_c	reference stress
$\theta^i_{\alpha j}$	($=\rho_{\alpha j}\omega^i_{\alpha j}$)mass of *i*-species in α–phase per unit volume of α–phase (*i*=*w,a;* α=*l,g;* *j*=1,2)	p_0	net mean yield stress at current suction and temperature
$\omega^i_{\alpha j}$	mass fraction of *i*-species in α–phase (*i*=*w,a;* α=*l,g;* *j*=1,2)	p^*_0	net mean yield stress for saturated conditions at reference temperature
ρ	parameter that relates cohesion and *T*	p^*_{0T}	net mean yield stress for saturated conditions at current temperature
ρ_s	solid density	$\mathbf{q}_{\alpha j}$	volumetric flux of α–phase with respect to the solid (α=*l,g;* *j*=1,2)
$\rho_{\alpha j}$	mass of α–phase per unit of volume of α–phase (α=*l,g;* *j*=1,2)	*r*	parameter defining the maximum macrostructural soil stiffness
$\boldsymbol{\sigma}_t$	total stress vector. $\{\sigma_x, \sigma_y, \sigma_z, \tau_{xy}, \tau_{xz}, \tau_{yz}\}^T_t$	$S_{\alpha j}$	volumetric fraction of pore volume occupied by α–phase (α=*l,g;* *j*=1,2)
$\boldsymbol{\sigma}$	net stress vector ($\boldsymbol{\sigma}_t - \mathbf{I}p_g$)	s_j	suction of medium *j* (p_g-p_{lj}; *j*=1,2)
ζ	parameter controlling the rate of increase of macrostructural soils stiffness with suction.	*T*	temperature (T_0 = reference temperature)
$\mathbf{D}_e$	elastic matrix	T_v	time factor
$\mathbf{D}_{ep}$	elasto-plastic matrix	*t*	Time
E_α	internal energy of α–phase per unit mass of α phase	**u**	solid displacement vector
$E^{\,i}_{\alpha j}$	internal energy of *i*-species in α–phase per unit mass of *i*-species (*j*=1,2)	u_j	excess pores pressures (*j*=1,2)
e_j	void ratio of medium *j* (*j*=1,2)	*V*, V_v	volume, volume of voids
F_{LC}	*BBM* yield surface	V_{v1}, V_{v2}	V_v of medium 1 and 2

Table 1. Main parameters of the elasto-plastic constitutive law presented in Section 4.1

Parameters defining the Barcelona Basic Model for macrostructural behavior								
κ_o	α_s	κ_s	μ	p_c (MPa)	r	ζ	$\lambda_{(0)}$	p_o^* (MPa)
0.125	-0.131	0.013	0.40	0.20	0.80	8.00	0.50	8.00
Parameters defining the law for microstructural behavior								
κ_{so}			α_s			χ		
0.125			-0.131			1		
Interaction function								
$f = -1 + 3\left(1 - p / p_o\right)^3$								

Table 2. Parameters related to the flow problem presented in Section 4.2

Parameters defining the retention curve				
P_{01} (MPa)	P_{02} (MPa)	$\lambda_{o1}=\lambda_{o2}$	$\lambda_{d1}=\lambda_{d2}$	$P_{d1} = P_{d2}$ (MPa)
50	1100	0.60	2.40	1100

Parameters defining the permeability law			
$k_{0\ 1}$ (m^2)	ϕ_o	b	n
$3.20\ 10^{-21}$	0.40	27	3

Leakage parameter (kg s^{-1} m^{-3} MPa^{-1}) = $4.0x10^{-7}$

Table 3. Main parameters of the elasto-plastic constitutive law presented in Section 5.1

Parameters defining the Barcelona Basic Model for macrostructural behavior										
κ_o	α_s	κ_s	μ	p_c (MPa)	r	ζ	$\lambda_{(0)}$	p_o^* (MPa)		
0.125	-0.137	0.013	0.40	0.20	0.80	8.00	0.50	10.0[(1)]	7.5[(2)]	5.5[(3)]
[(1)] ρ_d= 1.6 Mg/m^3; [(2)] ρ_d= 1.5 Mg/m^3; [(3)] ρ_d= 1.4 Mg/m^3										
Parameters defining the law for microstructural behavior										
α_m (MPa^{-1})				β_m (MPa^{-1})				χ		
2.0 e^{-02}				2.1 e^{-03}				1		
Interaction functions										
$f_C = 1 + 0.9\tanh\left(20\left(p / p_o\right) - 0.25\right)$ $f_S = 0.8 - 1.1\tanh\left(20\left(p / p_o\right) - 0.25\right)$										

Table 4. Main parameters of the elasto-plastic constitutive law presented in Section 5.1

Equation	Variable name	Equation	Parameter relationships	Parameters
Constitutive equations				
Darcy' laws	Liquid and gas advective flux	$\mathbf{q}_\alpha = -\mathbf{k}\ \frac{k_{r\alpha}}{\mu_\alpha}\left(\nabla P_\alpha - \rho_\alpha \mathbf{g}\right) \qquad \alpha = l, g$	$\mathbf{k} = k_0 \frac{\phi^3}{(1-\phi)^2}\frac{(1-\phi_0)^2}{\phi_0^3}\mathbf{I} \qquad k_{rl} = S_e^n$	k_0=1.9 e^{-21} m^2; n_0 = 0.40; n = 3
Fick's law	Vapour non advective flux	$\mathbf{i}_g^w = -\ \left(\ \phi\rho_g S_g \tau\, D_m^w \mathbf{I} + \rho_g \mathbf{D}_g^{'}\right)\ \nabla\omega_g^w$	$D_m^w = 5.9x10^{-12}\frac{(273.15+T)^{2.3}}{P_g}$	τ =0.8
Fourier's law	Conductive heat flux	$\mathbf{i}_c = -\lambda\nabla T$	$\lambda = \lambda_{sat}^{s_e}\lambda_{dry}^{(1-s_e)}$	λ_{sat}=1.15 λ_{dry}=0.47
Retention curve	Phase degree of saturation	$S_e = \left[1+\left(\frac{s}{P_o}\right)^{\frac{1}{1-\lambda_o}}\right]^{-\lambda_o}\left(1-\frac{s}{P_d}\right)^{\lambda_d}$	$S_e = \frac{S_l - S_{lr}}{S_{ls} - S_{lr}} \qquad S_l = 1 - S_g$	P_0=28 MPa; λ=0.18 P_d=1100MPa; λ_d=1.1
Mechanical Constitutive Model	Stress Tensor	$\dot{\boldsymbol{\sigma}} = \mathbf{D}_{ep}\cdot\dot{\boldsymbol{\varepsilon}} + \boldsymbol{\gamma}_s\dot{s} + \boldsymbol{\gamma}_T\dot{T}$; $\frac{\dot{p}_0^*}{p_0^*} = \frac{(1+e)}{(\lambda_{(0)}-\kappa)}\dot{\varepsilon}_v^p$ $\dot{\varepsilon}_v^e = \frac{\kappa}{(1+e)}\frac{\dot{p}}{p} + \frac{\kappa_s}{(1+e)}\frac{\dot{s}}{(s+0.1)} + (\alpha_0 + \alpha_2\Delta T)\dot{T}$	$F = \frac{3J^2}{g_y^{\,2}} - L_y^{\,2}(p+P_s)(P_o - p) = 0$; $p_0 = p_c\left(\frac{p_{0T}^*}{p_c}\right)^{\frac{\lambda_{(0)}-\kappa}{\lambda_{(s)}-\kappa}}$ $p_s = k_s\ e^{-\rho\Delta T}$; $p_{0T}^* = p_0^* + 2\left(\alpha_1\Delta T + \alpha_3\Delta T\left\lvert\Delta T\right\rvert\right)$ $\lambda_{(s)} = \lambda_{(0)}\left[r + (1-r)\exp(-\zeta s\ )\right]$ Mechanical model from Alonso et al. (1990) & Gens (1995)	κ=0.04; $\lambda_{(o)}$=0.14 P_o^*=14 MPa r=0.75; ζ=0.05 p_c=0.10MPa; M=1.5 k=0.1; ν=0.4 α_1=1.5x10^{-4} [1/C]; ρ=0.2
Phase density	Liquid density Gas density	$\rho_l = 1002.6\exp\left(4.5x10^{-4}\left(P_l - 0.1\right) - 3.4x10^{-4}T\right)$; ρ_g= ideal gas law		
Phase viscosity	Liquid viscosity Gas viscosity	$\mu_l = 2.1x10^{-12}\exp\left(\frac{1808.5}{273.15+T}\right)$; $\mu_g = 1.48x10^{-12}\exp\left(\frac{(273.15+T)^{1/2}}{1+\frac{119}{(273.15+T)}}\right)$		
Equilibrium restrictions				
Henry's Law	Air dissolved mass fraction	$\theta_l^a = \omega_a^l\rho_l = \frac{P_a}{H}\frac{M_a}{M_w}\rho_l$		
Psychometric Law	Water vapour dissolved mass fraction	$\theta_g^w = \left(\theta_g^w\right)^0\exp\left(\frac{\Psi M_w}{R(273.15+T)\rho_l}\right)$	$\left(\theta_g^w\right)^0 = \frac{M_w P_{v(T)}}{R(273.15+T)}$	

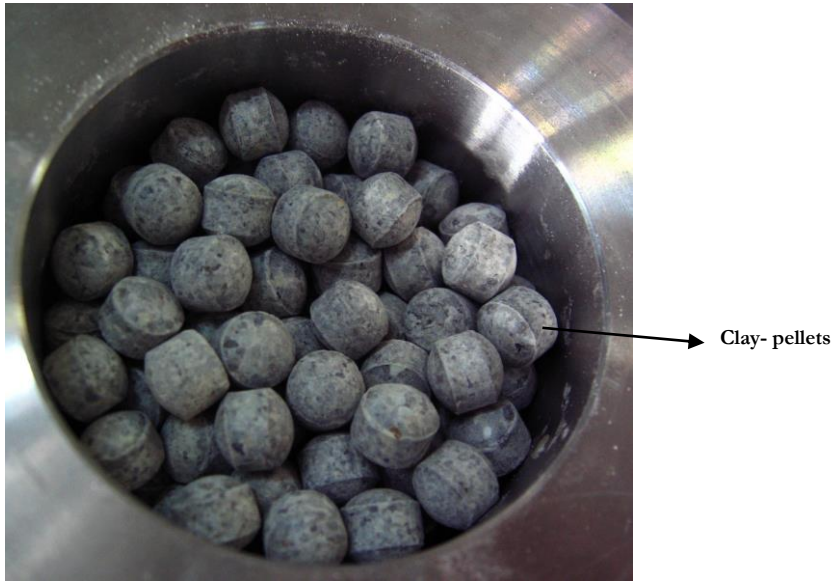

Figure 1. Clay-pellets.

Figure 2

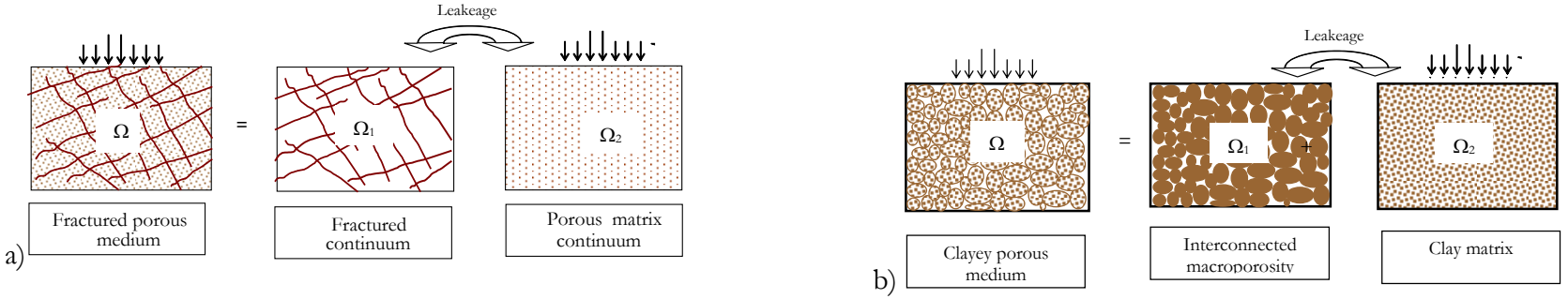

Figure 2. Schematic representation of double porosity concept, application to: a) fractured rocks, fissured clays (modified after Ghafouri and Lewis, 1996); b) expansive double structure clays.

Figure 3

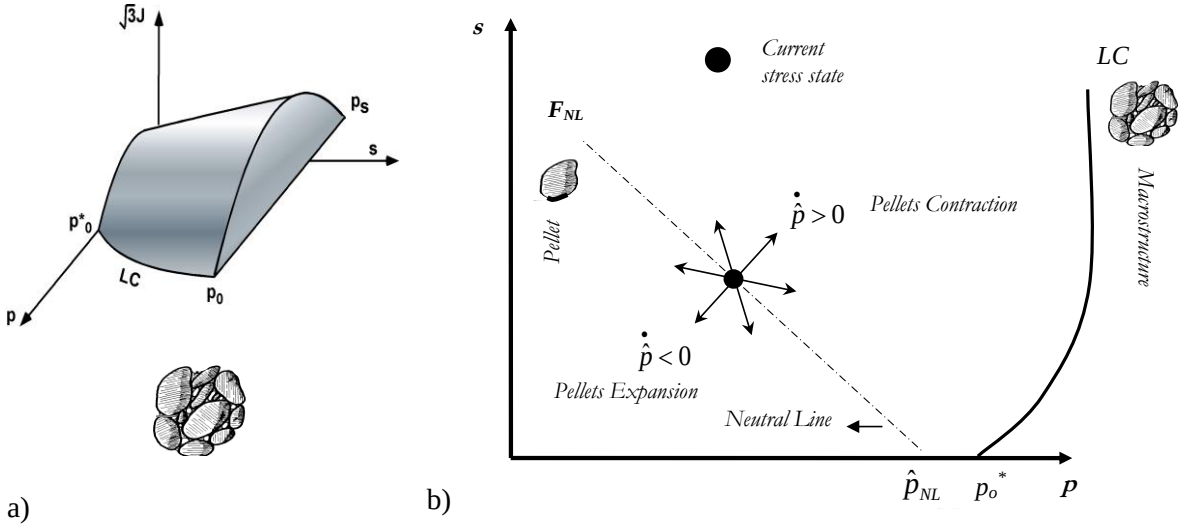

Figure 3.a) Three dimensional representation of the *BBM* yield surface adopted for the macrostructure.
b) Schematic representation of the expansive model on the *p-s* plane.

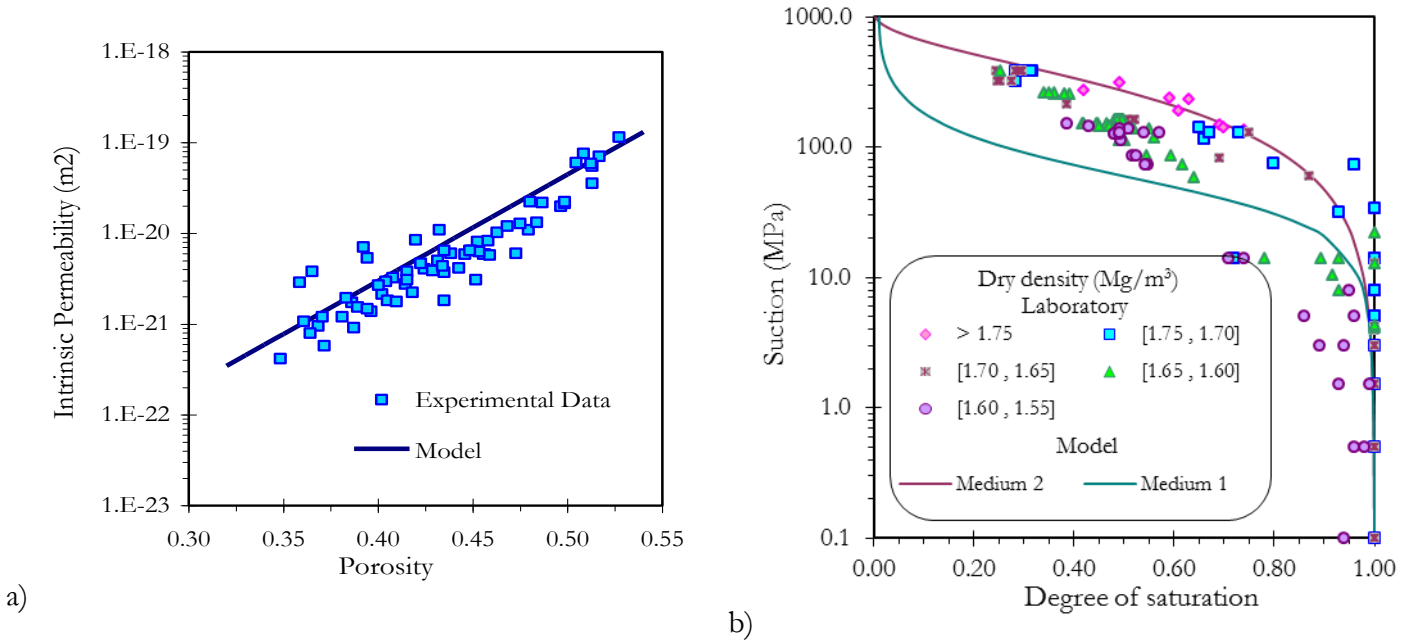

Figure 4. Serrata clay (also known as FEBEX bentonite): a) intrinsic permeability, and b) soil water retention curve (Huertas et al., 2000).

Figure 5

Click here to download Figure Figure 5-rev.doc

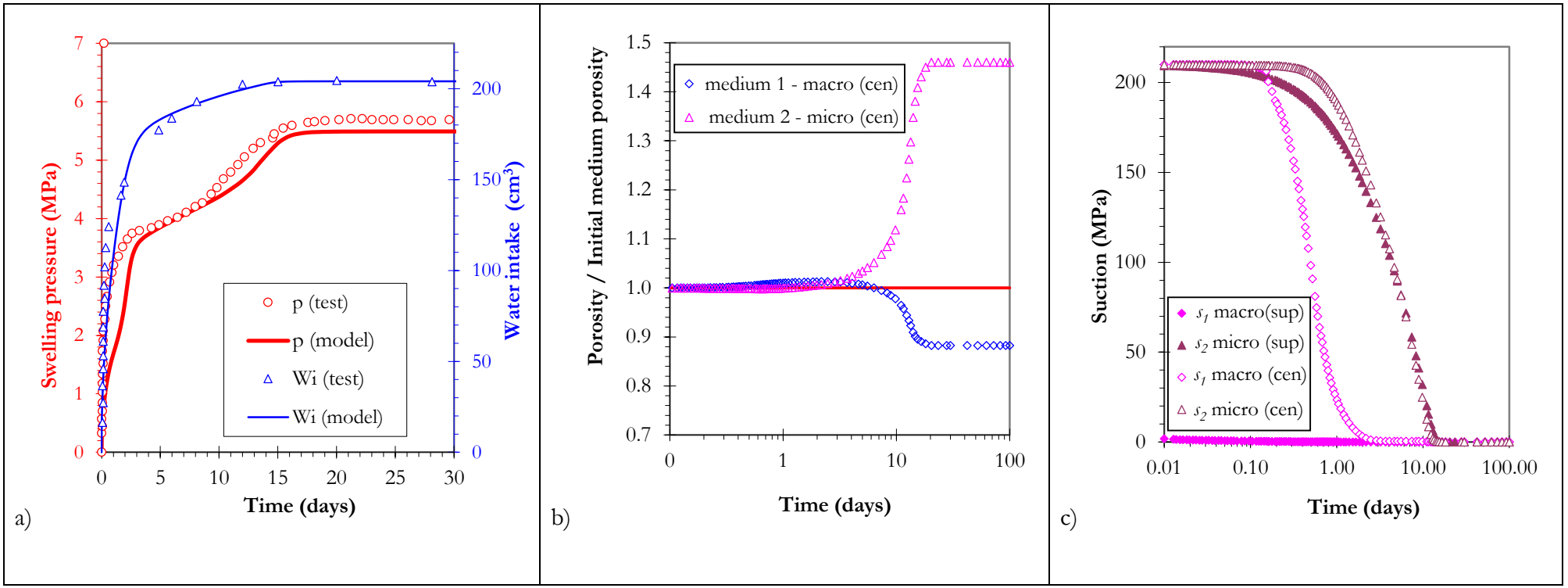

Figure 5. Swelling pressure test 'Reseal16' (experimental data from Volckaert et al., 2000): a) comparison of eexperimental data against numerical results in terms of swelling pressure and water intake versus time, b) evolution of macro and micro porosity at the center of the sample, c) time evolution of the suctions of in medium 1 and 2 (model results only).

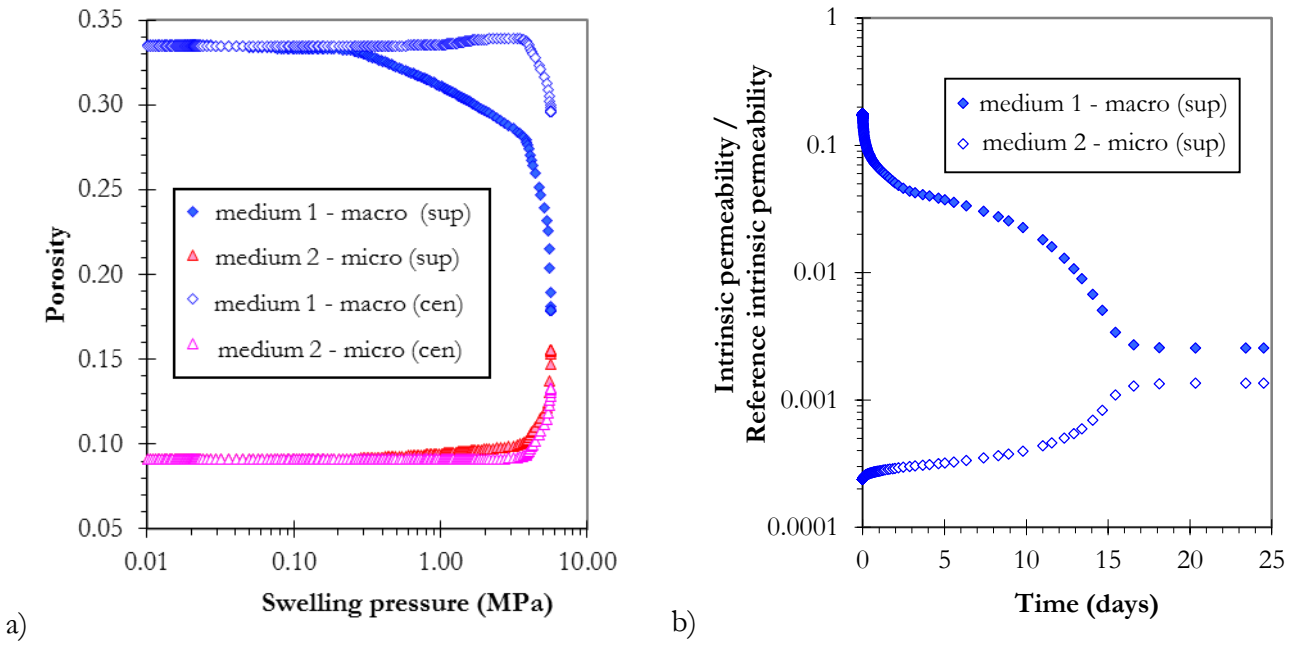

Figure 6. a) Evolution of intrinsic permeability in a zone close to the hydration boundary. b) Variation of porosity of medium 1 (macro) and 2 (micro) versus swelling pressure.

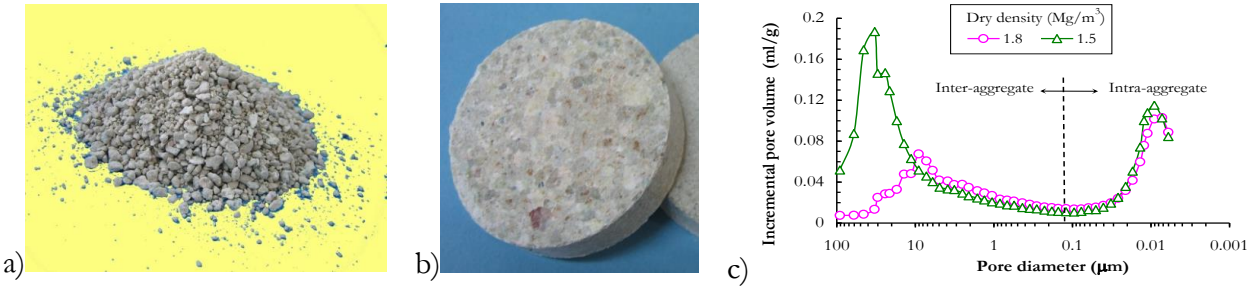

Figure 7. FEBEX bentonite: a) granulated raw material, and b) compacted sample, and c) mercury intrusion porosimetry tests of FEBEX bentonite (modified after Lloret et al., 2003).

a)

b)

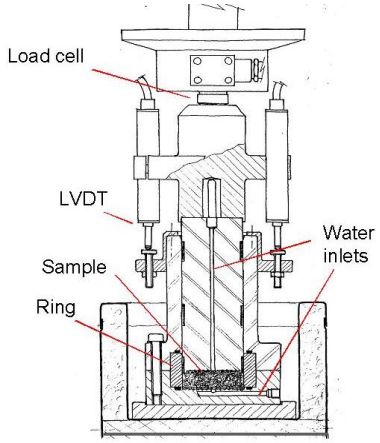

Figure 8 High-pressure oedometer: a) photo, and b) schematic representation showing its main components.

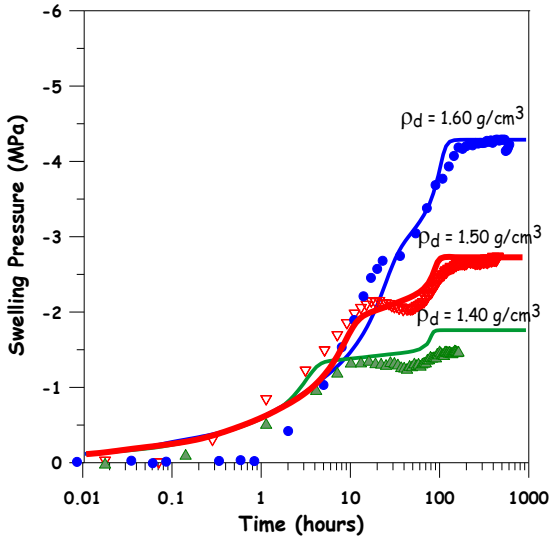

Figure 9. Evolution of swelling pressures tests at three different densities. Symbols represent experimental data and lines model results.

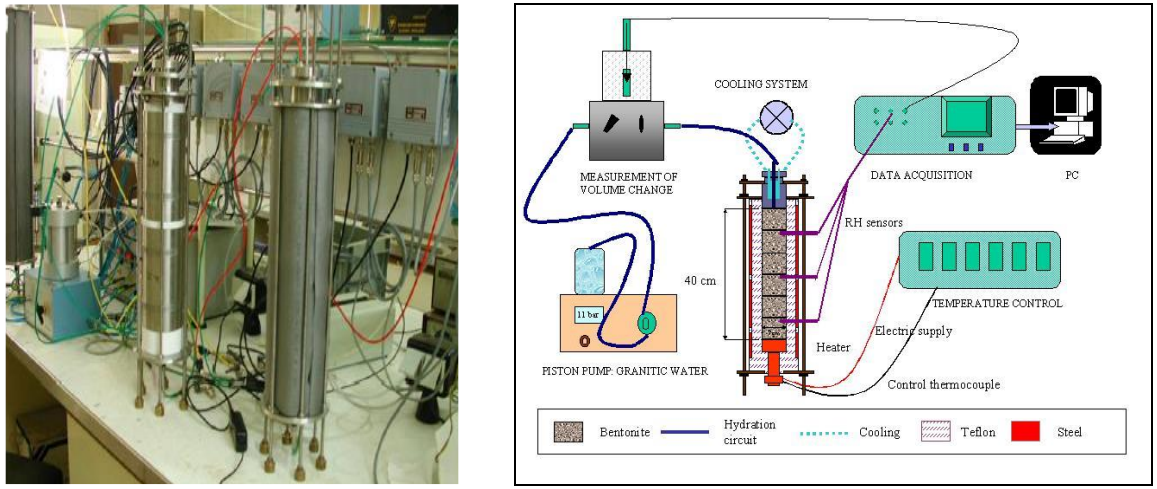

Figure 10. Infiltration cells: a) photo during operation, isothermal, I40 (left) and thermal gradient, GT40 (right); and b) experimental setup showing the main components.

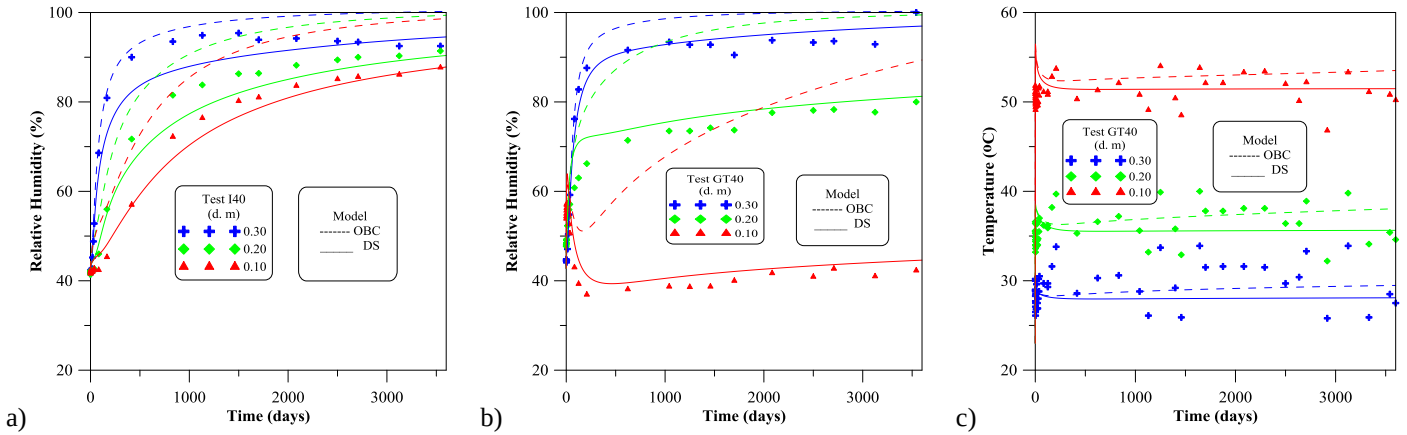

Figure 11. Plots showing experimental data and numerical results for the double structure (DS) and operational base case (OBC) models related to the cells GT40 and IT 40, results up to 10 years: a) time evolution of relative humidity cell IT40, b) time evolution of relative humidity of GT40; and c) time evolution of temperature GT40

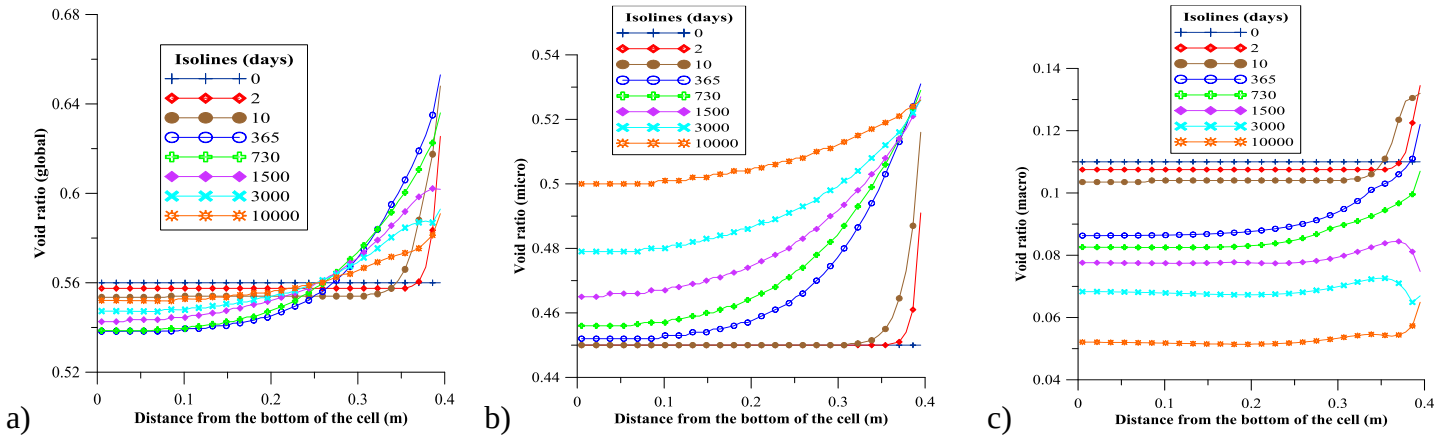

Figure 12. Evolution of different void ratio values along the cell at different times: a) global void ratio, b) micro void ratio, and c) macro void ratio.

Figures captions

Figure 1. Clay-pellets.

Figure 2. Schematic representation of double porosity concept, application to: a) fractured rocks, fissured clays (modified after Ghafouri and Lewis, 1996); b) expansive double structure clays.

Figure 3.a) Three dimensional representation of the *BBM* yield surface adopted for the macrostructure. b) Schematic representation of the expansive model on the *p-s* plane.

Figure 4. Serrata clay (also known as FEBEX bentonite): a) intrinsic permeability, and b) soil water retention curve (Huertas et al., 2000).

Figure 5. Swelling pressure test 'Reseal16' (experimental data from Volckaert et al., 2000): a) comparison of eexperimental data against numerical results in terms of swelling pressure and water intake versus time, b) time evolution of the suctions of in medium 1 and 2 (model results only), c) evolution of macro and micro porosity at the center of the sample.

Figure 6. a) Evolution of intrinsic permeability in a zone close to the hydration boundary. b) Variation of porosity of medium 1 (macro) and 2 (micro) versus swelling pressure.

Figure 7. FEBEX bentonite: a) granulated raw material, and b) compacted sample, and c) mercury intrusion porosimetry tests of FEBEX bentonite (modified after Lloret et al., 2003).

Figure 8 High-pressure oedometer: a) photo, and b) schematic representation showing its main components.

Figure 9. Evolution of swelling pressures tests at three different densities. Symbols represent experimental data and lines model results.

Figure 10. Infiltration cells: a) photo during operation, isothermal, I40 (left) and thermal gradient, GT40 (right); and b) experimental setup showing the main components.

Figure 11. Plots showing experimental data and numerical results for the double structure (DS) and operational base case (OBC) models related to the cells GT40 and IT 40, results up to 10 years: a) time evolution of relative humidity cell IT40, b) time evolution of relative humidity of GT40; and c) time evolution of temperature GT40

Figure 12. Evolution of different void ratio values along the cell at different times: a) global void ratio, b) micro void ratio, and c) macro void ratio.